REPORT

NEUROSCIENCE

Breathing control center neurons that promote arousal in mice

Kevin Yackle,[1]* Lindsay A. Schwarz,[2]† Kaiwen Kam,[3,4] Jordan M. Sorokin,[5] John R. Huguenard,[5] Jack L. Feldman,[3] Liqun Luo,[2] Mark A. Krasnow[1]‡

Slow, controlled breathing has been used for centuries to promote mental calming, and it is used clinically to suppress excessive arousal such as panic attacks. However, the physiological and neural basis of the relationship between breathing and higher-order brain activity is unknown. We found a neuronal subpopulation in the mouse preBötzinger complex (preBötC), the primary breathing rhythm generator, which regulates the balance between calm and arousal behaviors. Conditional, bilateral genetic ablation of the ~175 *Cdh9*/*Dbx1* double-positive preBötC neurons in adult mice left breathing intact but increased calm behaviors and decreased time in aroused states. These neurons project to, synapse on, and positively regulate noradrenergic neurons in the locus coeruleus, a brain center implicated in attention, arousal, and panic that projects throughout the brain.

Although breathing is commonly viewed as a simple autonomous function that sustains life, it has long been known to influence higher-order behavior and thinking (*1*). Slow, controlled breathing is used by practitioners of pranayama yoga and other forms of meditation to promote mental calming and contemplative states, and it is used clinically to suppress excessive arousal and stress such as certain types of panic attacks (*2*, *3*). Although the effect of breathing on behavior and mental state could easily be indirect, there could also be more direct connections and impact of the breathing center on higher-order brain function (*4*), as demonstrated here.

The preBötzinger complex (preBötC) is a cluster of several thousand neurons in the ventrolateral medulla of the murine brain that can autonomously generate respiratory rhythms in explanted brain slices (*5*, *6*), and whose rhythmic activity in vivo initiates breathing by recurrently activating premotor and motor neurons of the respiratory muscles (*5*). The preBötC is not a homogeneous population of neurons but is composed of distinct, though intermingled, neuronal subpopulations (*5*, *7*), one of which is essential for respiratory-rhythm generation (*8*, *9*) and another for sighing (*10*).

To systematically explore the molecular diversity of breathing center neurons, we screened expression patterns of over 19,000 genes in the Euroexpress embryonic day 14.5 (E14.5) mouse hindbrain database (*11*). Cadherin-9 (*Cdh9*) was the gene most selectively expressed in preBötC (Fig. 1A). We constructed a bacterial artificial chromosome (BAC) transgene with the mOrange coding sequence inserted at the *Cdh9* translation start codon (Fig. 1B). Cell counts in early postnatal brains detected 319 ± 130 (n = 6) Cdh9-mOrange–expressing cells in preBötC (Fig. 1C). These cells intermingled with neurons expressing canonical preBötC markers somatostatin (SST) and neurokinin 1 receptor (NK1R) (Fig. 1, D and E, and fig. S1, A to E). Few expressed the markers themselves: 0 out of 43 Cdh9-mOrange+ cells scored were SST+, and 7 out of 179 Cdh9-mOrange+ (4%) were NK1R+. All Cdh9-mOrange–expressing cells coexpressed neuronal marker NEUN (n = 61 cells, Fig. 1F). These Cdh9-mOrange–expressing neurons can be further divided into seven subtypes based on differential expression of transcription factors *Pax2*, *Dach1*, *Lmo4*, *Evx1*, and *Dbx1*. We focused on the ~175 neurons in each preBötC (fig. S1, F to J; ~350 neurons bilaterally) that coexpress the *Dbx1*-lineage marker, the major subpopulation (56%, 165 out of 292 scored Cdh9-mOrange+ cells, were Dbx1-LacZ+) we call *Cdh9*/*Dbx1* neurons (Fig. 1, G to I).

We electrophysiologically recorded 26 mOrange-positive neurons in 15 preBötC slice preparations from Cdh9-mOrange;Dbx1-lacZ double-transgenic postnatal day 0 to 5 (P0 to P5) mice, then post-stained the neurons for β-galactosidase (LacZ) in some preparations to identify recordings of *Cdh9*/*Dbx1* neurons (table S1). We definitively identified five *Cdh9*/*Dbx1* neurons. One showed bursts of action potentials just before or during each preBötC inspiratory burst (Fig. 1J and fig. S2), like most other *Dbx1*-lineage preBötC neurons (*12*). Three other neurons were more broadly active with bursts during some, but not all, preBötC inspiratory bursts (42, 41, and 88% of inspiratory bursts; Fig. 1K and fig. S2), called an "inspiratory-associated" activity pattern. The other neuron showed sporadic activity with no apparent relationship to preBötC inspiratory bursts. Seven of the 15 Cdh9-mOrange neurons whose Dbx1-lacZ expression status was not determined also displayed inspiratory (four neurons) or inspiratory-associated (two neurons) patterns (table S1).

We used intersectional genetics (Cdh9-LOSL-DTR;Dbx1-cre) (Fig. 1, B, M, and N) to express human diphtheria toxin receptor (DTR) only in *Dbx1*-lineage cells that coexpress *Cdh9*, so that *Cdh9*/*Dbx1* neurons could be specifically ablated by intraperitoneal injection of diphtheria toxin. We expected there would be few, if any, cells besides *Cdh9*/*Dbx1* preBötC neurons that express both genes (*11*, *13*). We examined this in two ways. First, we compared mOrange expression in Cdh9-LOSL-DTR and Cdh9-LOSL-DTR;Dbx1-cre transgenic mice by immunostaining serial sections of adult brains. The only regions where Dbx1-cre reduced the number of mOrange-expressing cells were preBötC and inferior colliculus (fig. S3). Co-staining with other markers showed that loss of mOrange in preBötC was specific and complete for *Cdh9*/*Dbx1* neurons and had little or no effect on the six other (*Dbx1*-negative) *Cdh9*-positive preBötC cell types (fig. S4). Second, immunostaining of serial sections of Cdh9-LOSL-DTR;Dbx1-cre adult brains detected DTR expression only in *Cdh9*/*Dbx1* preBötC neurons (Fig. 1M) and the inferior colliculus (fig. S3). Intraperitoneal injection of diphtheria toxin once a day for 3 days eliminated the DTR-expressing cells (Fig. 1N).

We analyzed adult mice several days after ablating *Cdh9*/*Dbx1* neurons. We expected *Cdh9*/*Dbx1* neurons would be essential for breathing and viability because *Dbx1* neurons are essential for breathing in vivo (*8*, *9*) and ablating just 85 random *Dbx1* neurons abolishes preBötC rhythms in vitro (*14*). However, there was no overt effect on viability (three of three scored mice alive >1 year after ablation), breathing, or sensory and motor behaviors. Plethysmography of freely moving adult mice after ablation did not detect significant differences in inspiratory time, expiratory time, or tidal volume of standard (eupneic) breaths (figs. S5A and S6). No differences were detected in characteristics of four variant breath types (figs. S5, B to E, and S6) or breaths during sleep or under hypercapnic or hypoxic conditions (figs. S5, F to H, and S6).

There was, however, a change in abundance of different breath types, first noted in respiratory-rate histograms: *Cdh9*/*Dbx1* ablation shifted the distribution toward slower breaths (low respiratory rate) (Fig. 2B). Inspection of plethysmograph traces indicated that the shift was due to increased slow breaths (eupneic and grooming) associated with calm behaviors and reduction in rapid breaths associated with sniffing and other active behaviors (Fig. 2A and fig. S7).

[1]Howard Hughes Medical Institute, Department of Biochemistry, Stanford University School of Medicine, Stanford, CA 94305, USA. [2]Howard Hughes Medical Institute, Department of Biology, Stanford University, Stanford, CA 94305, USA. [3]Systems Neurobiology Laboratory, Department of Neurobiology, David Geffen School of Medicine, University of California–Los Angeles, Los Angeles, CA 90095, USA. [4]Department of Cell Biology and Anatomy, Chicago Medical School, Rosalind Franklin University of Medicine and Science, North Chicago, IL 60064, USA. [5]Department of Neurology and Neurological Sciences, Stanford University, Stanford, CA 94305, USA.
*Present address: Department of Physiology, University of California–San Francisco, San Francisco, CA 94158, USA.
†Present address: Department of Developmental Neurobiology, St. Jude Children's Research Hospital, Memphis, TN 38105, USA.
‡Corresponding author. Email: krasnow@stanford.edu

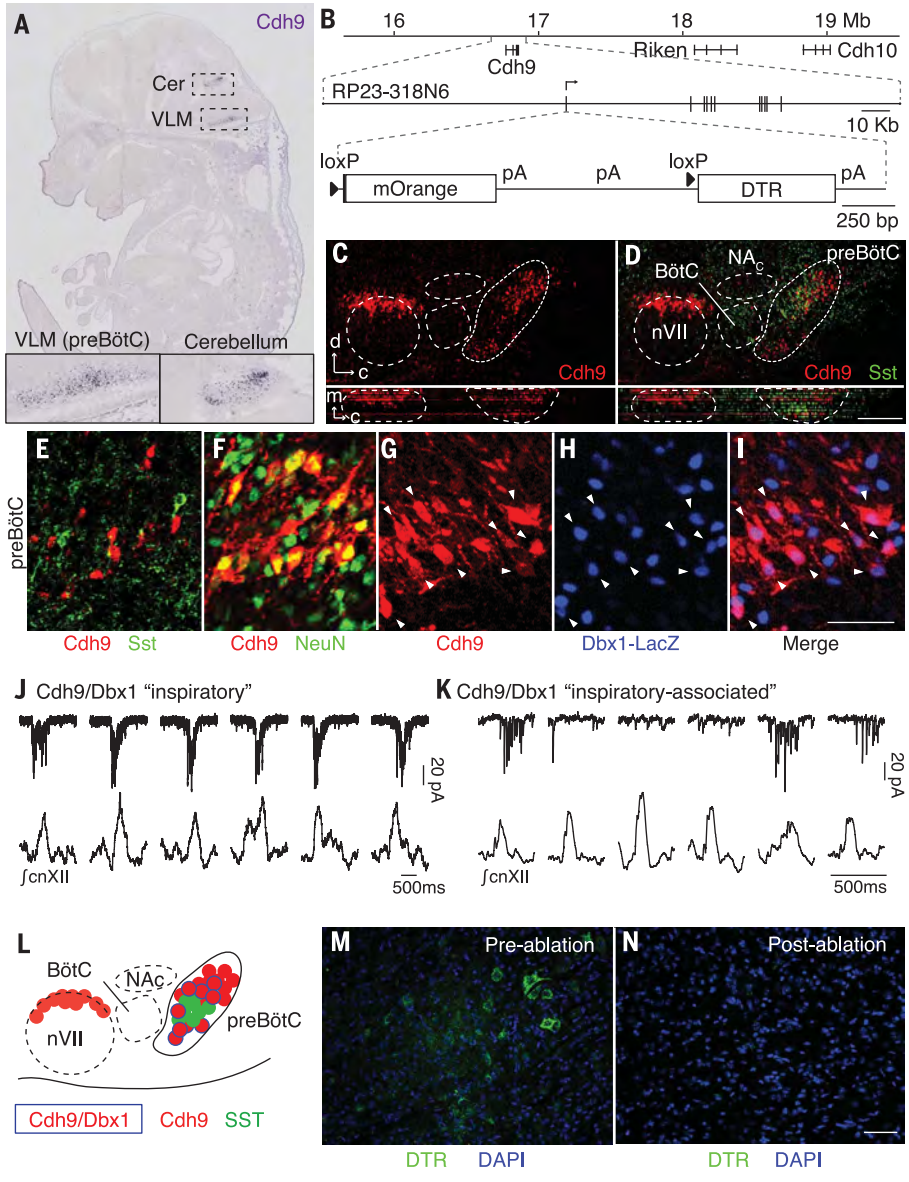

Fig. 1. Identification and genetic ablation of *Cdh9/Dbx1* double-positive neurons in preBötC. (**A**) *Cdh9* mRNA expression (blue) in section of E14.5 mouse embryo (*11*). Insets, ventrolateral medulla (VLM) and ventral cerebellum (Cer). (**B**) (Top) *Cdh9* locus on Chromosome 15 (numbers indicate distance from centromere). (Middle) BAC RP23-318N6. Vertical lines indicate *Cdh9* exons. (Bottom) Cdh9-LOSL-DTR BAC transgene: insertion at *Cdh9* start codon of mOrange sequence and polyadenylation (pA) signals, flanked by *loxP* sites (triangles), followed by DTR sequence. (**C** and **D**) VLM sections of P0 Cdh9-LOSL-DTR mouse immunostained for mOrange to show *Cdh9* expression (red) and P0 wild-type mouse immunostained for somatostatin (SST, green), shown aligned [registered by compact nucleus ambiguus (NA_C), cranial nerve 7 (nVII), and ventral brainstem surface] in sagittal plane (upper panels) and transverse projection (lower panels). d, dorsal; c, caudal; m, medial. Scale bar, 200 μm. (**E** to **I**) preBötC of a P0 Cdh9-LOSL-DTR [(E) and (F)] or Cdh9-LOSL-DTR;Dbx1-lacZ [(G) to (I)] mouse immunostained for Cdh9-mOrange [(E) to (G) and (I), red], SST [(E), green], NEUN [(F), green], or β-galactosidase [*Dbx1*-LacZ, (H) and (I), blue]. Among *Cdh9*-expressing neurons, none coexpressed SST (n = 43 cells), all coexpressed NEUN (n = 57), and 56% coexpressed *Dbx1* reporter (n = 292, arrowheads). Scale bar [(E) to (I)], 50 μm. (**J** and **K**) Whole-cell voltage-clamp recordings of *Cdh9/Dbx1* preBötC neurons in slice *Cdh9* preparations (top) and simultaneous integrated cranial nerve 12 (cnXII) activity (bottom). Neuron in (J) (neuron 1, table S1) shows bursts in all inspiratory events (inspiratory pattern). Neuron in (K) (neuron 3) shows more widespread activity but bursts only during some events (inspiratory-associated). Scale bars, 500 ms. (**L**) Schematic of VLM. *Cdh9/Dbx1* neurons (blue border) intermingle with SST (green) and other *Cdh9* neurons (red) in preBötC. (**M** and **N**) Intersectional genetic labeling of *Cdh9/Dbx1* preBötC neurons with DTR (immunostain, green) in ~P35 Cdh9-LOSL-DTR;Dbx1-cre mice before (M) and after (N) intraperitoneal DT injection to ablate them. Scale bar, 50 μm.

The change in breathing patterns after *Cdh9/Dbx1* neural ablation was accompanied by a corresponding change in behavior. Ablation reduced exploration of a new environment (87 ± 9% versus 62 ± 20% time spent in active exploration, pre- versus postablation; P = 0.02) and increased time engaged in grooming threefold (10 ± 7% versus 31 ± 16%; P = 0.02) and still-sitting twofold (3 ± 4% versus 7 ± 7%; P = 0.07), although the latter did not reach statistical significance (Fig. 2C). There was an increase in both number of calm episodes (Fig. 2D) and their duration (Fig. 2E and movie S1). Because the breathing pattern associated with each behavioral state was not detectably altered by ablation (figs. S5 and S6), the observed change in respiratory-rate distribution could be explained by the overall change in behavior (fig. S8): a shift from active toward calm behaviors. Electrocorticographic (ECoG) monitoring showed an increase in slow-wave (delta, 2 to 4 Hz) brain activity after ablation (Fig. 2F) and a selective decline in time spent in an active-brain state dominated by theta activity (Fig. 2G) compared to that of littermate controls (Fig. 2, H and I). These changes could be temporarily reversed by illuminating the chamber, providing a stimulus that apparently overrides the decrease in arousal caused by *Cdh9/Dbx1* ablation (fig. S9).

To confirm that the observed behavioral and breathing changes were due to ablation of neurons in the preBötC, we restricted DTR induction and hence neural ablation to just *Cdh9*-expressing preBötC neurons (fig. S10, A to C). The animals displayed a diminution in active exploratory behaviors and breathing patterns and an increase in calm behaviors and breathing patterns similar to animals with *Cdh9/Dbx1* neurons ablated using our intersectional genetic strategy (compare fig. S10, D and E, and Fig. 2).

The decrease in active behavior and increase in ECoG delta waves observed after *Cdh9/Dbx1* neuron ablation is reminiscent of changes following silencing or ablation of the locus coeruleus (LC), a noradrenergic nucleus in the pons implicated in generalized arousal, stress, and sleep-wake transitions (*15*). We thus microinjected two retrograde tracers into the LC and found that both labeled Cdh9-mOrange neurons in preBötC (FluorGold: fig. S11, A to C; fluorescent retrograde beads: data not shown). Most of the labeled Cdh9-mOrange preBötC neurons (85%, 23 out of 27, n = 40 sections, 3 mice) were contralateral to the injection site. The connection is selective because most labeled preBötC neurons expressed Cdh9-mOrange (72%, 13 out of 18, n = 10 sections, 4 mice), and no retrograde labeling of Cdh9-mOrange neurons was observed following tracer injection into regions surrounding the LC (n = 4 injections).

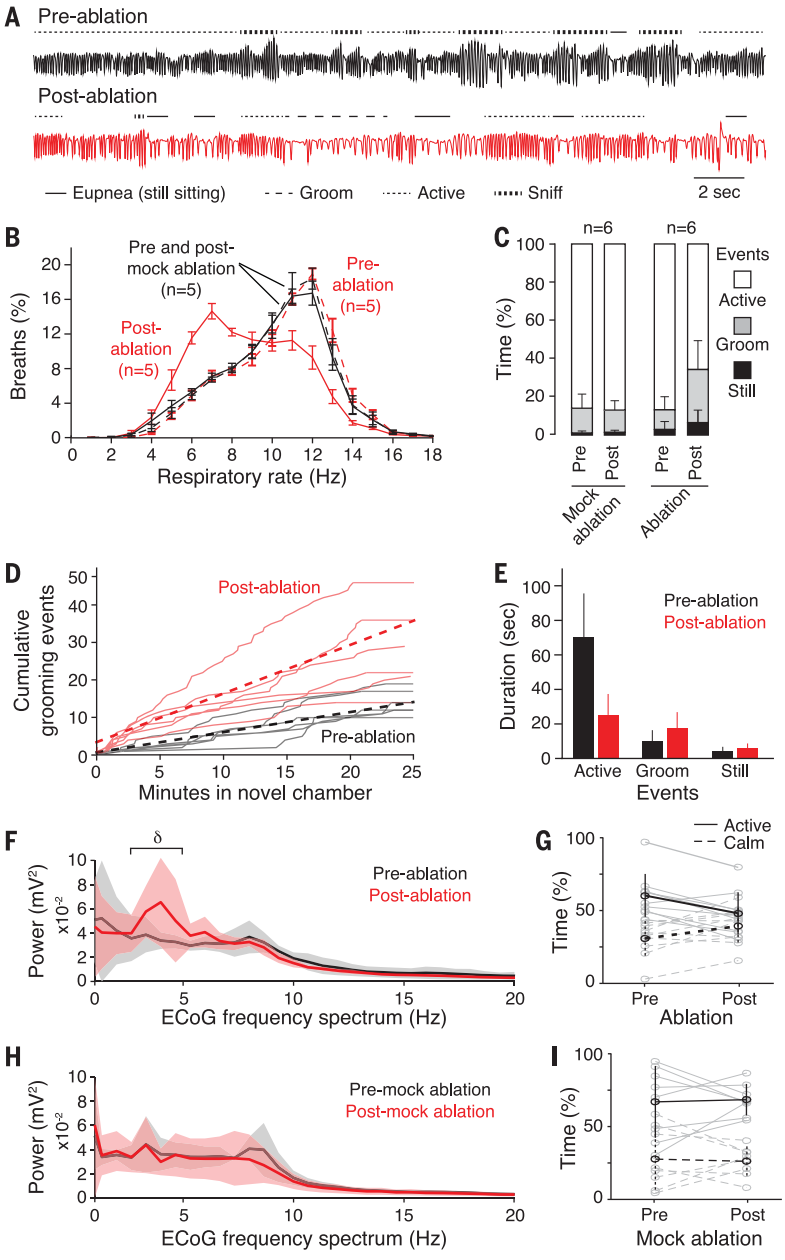

Fig. 2. Respiratory and behavior changes after *Cdh9/Dbx1* neuron ablation. (**A**) Plethysmography airflow traces of Cdh9-LOSL-DTR;Dbx1-cre mice before (black) and 2 days after (red) *Cdh9/Dbx1* ablation. Note increased grooming and eupneic breaths and decreased active breaths and sniffing after ablation (see key). Scale bar, 2 s. (**B**) Distribution of respiratory rates (bin size 1 Hz) in 40-min assay of control (wild-type, Cdh9-LOSL-DTR, or Dbx1-cre; black, n = 5) and experimental (Cdh9-LOSL-DTR; Dbx1-cre; red, n = 5) animals before (dashed lines) and 2 days after (solid lines) *Cdh9/Dbx1* ablation. (**C**) Percent of time in plethysmography chamber spent still-sitting (black), grooming (gray), or active (white) by control (n = 6) or experimental (n = 6) mice before (pre) or 2 days after (post) ablation or mock ablation. P values comparing pre- and postablation behavior: active (0.02), grooming (0.02), and still-sitting (0.07). (**D**) Grooming events in new chamber of Cdh9-LOSL-DTR;Dbx1-cre mice before (black) or after (red) ablation. Solid lines, individual mice (n = 6); dashed lines, average. (**E**) Duration of behaviors in (C) (mean ± SD, n = 6). After ablation, active episodes shortened (P = 0.005), grooming and still-sitting showed nonsignificant trend to lengthening (P = 0.24 and 0.21, respectively). (**F** and **H**) ECoG power spectral analysis [average (solid lines) ± SEM] of 20-min recording (trial 1) of Cdh9-LOSL-DTR;Dbx1-cre [(F), n = 5] or control Cdh9-LOSL-DTR [(H), n = 4] mice before (black) or 4 to 10 days after (red) ablation. δ, delta wave; V, voltage. Active behavior correlates with faster breathing (fig. S15, C to E). (**G** and **I**) Time spent in active (solid black line, mean ± SEM) and calm (dashed black line) behavioral states defined by electromyography (EMG) and ECoG (fig. S15) of individual animals in (F) and (H) (gray lines) during two 20-min assays pre- and post-*Cdh9/Dbx1* ablation. Note decreased active and increased calm periods following ablation in experimental animals (P = 0.001 and 0.02, respectively, paired t test) and no change in controls (P = 0.86 and 0.81, respectively).

We tested whether the observed connection between the preBötC neurons and LC is direct to the noradrenergic [dopamine β-hydroxylase (*Dbh*)–expressing] neurons that dominate the LC (*15*). Injection of Cre-dependent adeno-associated virus (AAV) helper viruses (AAV-FLEx^{loxP}-TVA: mCherry and AAV-FLEx^{loxP}-rabies glycoprotein), which enables infection and monosynaptic spread of an envA-pseudotyped, glycoprotein-deleted, and GFP-expressing rabies virus (RVdG) (*16*), into the LC of Dbh-cre;Cdh9-mOrange mice resulted in specific infection of LC "starter" neurons by RVdG (fig. S12) and selective retrograde transsynaptic tracing (GFP-labeling) of Cdh9-mOrange neurons in the preBötC (Fig. 3, A to D, and fig. S11, D to F). We again observed a strong bias for labeling the contralateral rather than ipsilateral preBötC (compare Fig. 3, A to C, and fig. S11, D to F). Most of the green fluorescent protein (GFP)–labeled neurons in the contralateral preBötC (63%, 45 out of 72, n = 18 sections, 3 mice) expressed Cdh9-mOrange, whereas few of the labeled ipsilateral preBötC neurons expressed Cdh9-mOrange (7%, 7 out of 94, n = 18 sections, 3 mice). Nearly all ipsilateral GFP-expressing neurons were located outside the canonical preBötC region defined by SST expression, so they are presumably not preBötC neurons (fig. S13). Control experiments in mice without Dbh-cre did not show double-positive preBötC neurons (fig. S12).

We microinjected a retrogradely transported *cre*-expressing virus, canine adenovirus type 2–Cre (CAV-Cre), bilaterally into the LC of Cdh9-LOSL-DTR mice to eliminate mOrange and express DTR only in the *Cdh9*-expressing neurons that project to LC (Fig. 3E). Before DT injection, animals breathed and behaved normally, although there was an increase in calm breathing relative to mock-ablated controls, perhaps because of neural toxicity associated with induced DTR expression (Fig. 3, H and I). Four to 10 days after DT injection and ablation of LC-projecting, *Cdh9*-expressing preBötC neurons (Fig. 3, F and G), there was a change in breathing (Fig. 3H) and decrease in active behaviors (Fig. 3I) that mimicked those observed after ablation of the *Cdh9/Dbx1* preBötC neurons (compare to Fig. 2, B and C).

We examined LC activity by c-FOS expression (*17*) following *Cdh9/Dbx1* neuron ablation. Under standard housing conditions, Cdh9-LOSL-DTR; Dbx1-cre littermate control mice with intact *Cdh9/Dbx1* neurons showed only occasional LC activity (Fig. 4, A and D, and fig. S14). When animals were placed in a new environment (plethysmography

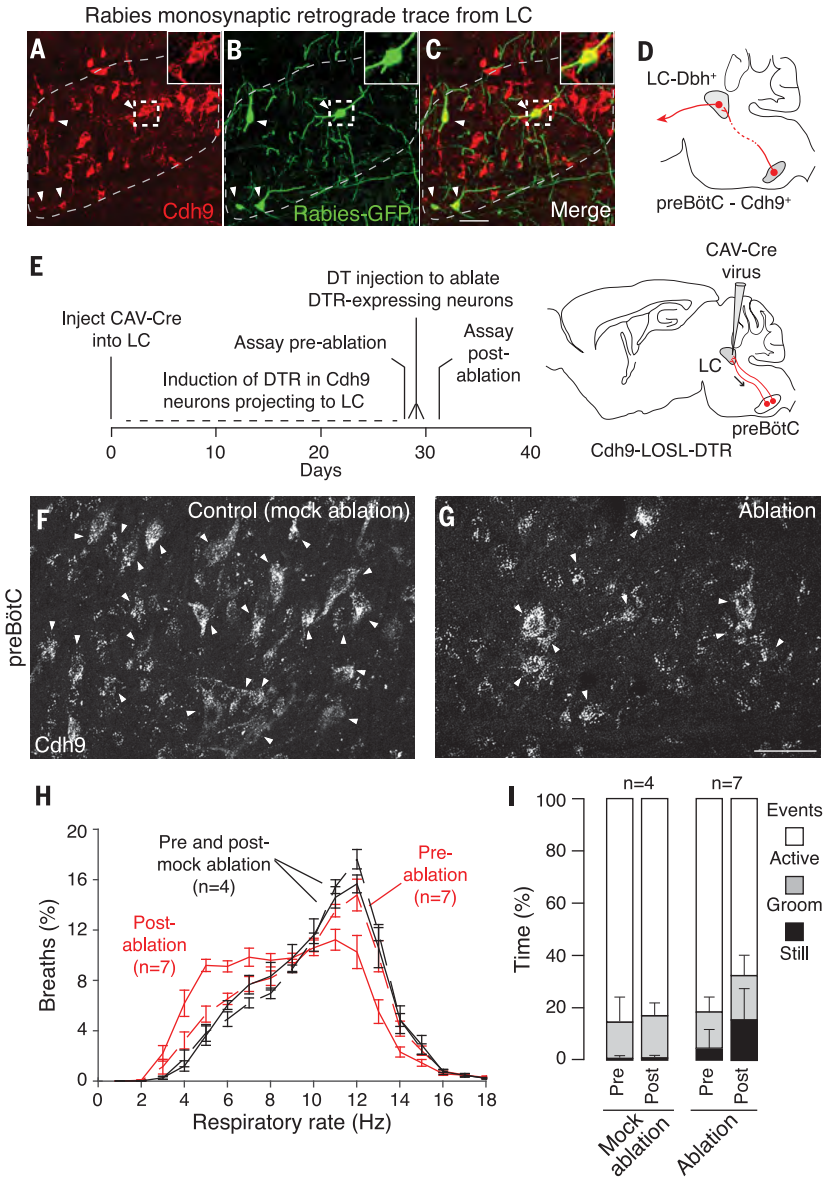

Fig. 3. Effect on breathing and behavior of ablation of *Cdh9* neurons that project to and synapse on LC neurons. (**A** to **D**) Rabies virus monosynaptic retrograde trace from dopamine β-hydroxylase (*Dbh*)–expressing locus coeruleus (LC) neurons. Section through contralateral preBötC (A) to (C) of adult Cdh9-LOSL-DTR;Dbh-cre mouse 5 days after unilateral LC injection of rabies-GFP and helper virus, immunostained to show *Cdh9*-expressing neurons (mOrange, red). Arrowheads indicate colocalization of GFP and mOrange. Insets highlight boxed region. Scale bar, 50 μm. (D) Schematic of monosynaptic projection (red line) from *Cdh9*-expressing preBötC neurons (red circle) to contralateral LC, which projects to higher brain structures (arrow). (**E**) Scheme for ablating only *Cdh9*-expressing preBötC neurons that project to LC. CAV-Cre virus injected bilaterally into LC of adult Cdh9-LOSL-DTR mice (right) is taken up by *Cdh9*-expressing preBötC neurons that project there (red). Cre induces DTR expression, and DT injection induces ablation. (**F** and **G**) preBötC Cdh9-mOrange expression (white) in control uninjected [(F), mock ablation] and CAV-Cre injected [(G), ablation] Cdh9-LOSL-DTR mice 2 days after DT injection. Scale bar, 50 μm. Quantification showed 32% (mean) and 50% (maximal) reduction in mOrange neurons (n = 15 sections), close to the value expected if all *Cdh9/Dbx1* preBötC neurons (50% of *Cdh9*-expressing neurons) project to LC. (**H**) Distribution of respiratory rates in 40-min assay (as in Fig. 2B) of CAV-Cre injected Cdh9-LOSL-DTR adult mice (red, n = 7) or wild-type littermates (black, n = 4) before (dashed) and 2 days after (solid) DT injection. (**I**) Behavioral analysis (as in Fig. 2C) of mice in (H). Pre- versus postablation P values: active (0.015), grooming (0.37), and still-sitting (0.015). The increased calm events in preablation experimental versus control mice was reproducible; it may be due to toxicity of DTR induced in adult neurons, which is not observed in Cdh9-LOSL-DTR;Dbx1-cre mice when DTR is expressed in early development, perhaps due to developmental compensation.

chamber) for 1 hour, c-FOS was induced in scattered cells throughout the LC (Fig. 4, B and D, and fig. S14). However, 4 days after *Cdh9/Dbx1* neuron ablation, only rare c-FOS–positive LC neurons were detected before or after placement in the chamber (Fig. 4, C and D, and fig. S14). The LC of ablated animals remained responsive to the extreme arousal stimulus of physical-restraint stress (*18*) (Fig. 4, D to F, and fig. S13), indicating that other LC inputs and functions were intact.

We have identified and characterized a new neuronal subtype in the preBötC comprising ~175 of its ~3000 neurons. The *Cdh9/Dbx1* neurons are dispensable for respiratory-rhythm generation and instead promote generalized behavioral arousal. Ablation of these neurons left all major breathing patterns and regulation intact but made the mice preternaturally calm: Their activity and ECoG profiles shifted from active exploratory behavior and brain wave patterns toward calm behaviors such as still-sitting and grooming. Monosynaptic tracing demonstrated that these neurons directly project to and synapse on noradrenergic neurons in the contralateral LC, which in turn project throughout the brain and control generalized arousal and sleep-wake transitions (*15*). *Cdh9/Dbx1* preBötC neurons provide excitatory input to the LC and appear to be the dominant activating input under mild arousal conditions of placement in a new chamber.

We propose that *Cdh9/Dbx1* preBötC neurons function as gateway neurons directly linking the preBötC to the locus coeruleus, and through it to the rest of the brain (Fig. 4G). This ascending circuit allows the respiratory center to communicate directly with and control higher-order brain structures associated with behavioral arousal. The excitatory input to the LC is presumably provided by the observed inspiratory-associated activity patterns of *Cdh9/Dbx1* neurons, which could provide greater excitatory input with faster respiratory rates and perhaps abnormal respiratory patterns (Fig. 4H). This respiratory corollary signal would thus serve to coordinate the animal's state of arousal with the breathing pattern, leaving the animal calm and relaxed when breathing is slow and regular, but promoting (or maintaining) arousal when breathing is rapid or disturbed. This circuit and corollary signal would explain why preBötC respiratory patterns have been observed in the LC and other reticular activating structures (*19*–*21*). The LC can increase respiratory rate (*22*), so there may also be a positive feedback loop from the LC ultimately back to *Cdh9/Dbx1* preBötC neurons.

The *Cdh9/Dbx1* circuit may have evolved as a defense response, mobilizing the animal in the face of rapid, irregular, or labored breathing. Indeed, fast or erratic breathing in humans increases alertness and can cause anxiety and even panic (*3*), and likewise increased preBötC activity, hyperventilation, and sighs appear to induce arousal during sleep (*23*–*25*). Conversely, slow and controlled breathing has long been known by practitioners of

pranayama yoga to induce relaxation, and related approaches have proven useful for anxiety syndromes and other stress disorders (*1*, *2*). If the *Cdh9/Dbx1* circuit is conserved in humans, it could provide a therapeutic target for breathing-related anxiety disorders and perhaps prevention of sudden infant death syndrome (SIDS), widely hypothesized to result from an inadequate arousal response to asphyxiation during sleep (*24*).

Notably, panic attacks triggered by respiratory symptoms are specifically responsive to clonidine, an α2-adrenergic agonist that silences LC (*26*).

Although breathing is generally thought of as an autonomic behavior, higher-order brain functions can exert exquisite control over breathing. Our results show, conversely, that the breathing center has a direct and powerful influence on higher-order brain function. It will thus be important to map the full range of behaviors and functions the breathing center controls.

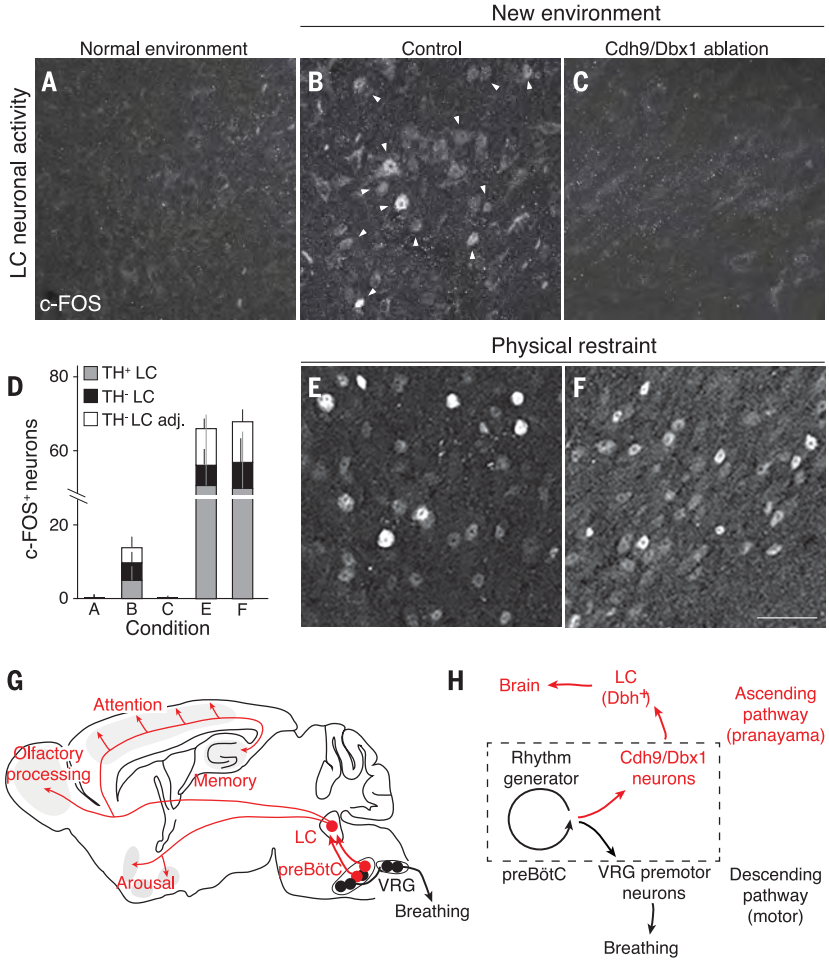

Fig. 4. Effect of *Cdh9/Dbx1* neuron ablation on LC neuronal activity. (**A** to **C**, **E**, and **F**) c-FOS immunostaining (arrowheads) in LC of adult wild-type mouse in normal environment [home cage, (A)] and of control [wild-type, Cdh9-LOSL-DTR, or Dbx1-cre mice, (B) and (E)] and *Cdh9/Dbx1*-ablated mice [Cdh9-LOSL-DTR;Dbx1-cre mice 2 days after DT injection, (C) and (F)] after 1 hour in new chamber [(B) and (C)] or in a conical tube under physical restraint [(E) and (F)]. Scale bar, 50 μm. (**D**) Quantification of c-FOS$^+$ neurons in (A) to (C) and (E) and (F) (mean ± SD) per 25-μm section of LC: (A) 0.4 ± 0.8 neurons (n = 39 sections, 6 animals); (B) 13.8 ± 6.5 neurons (14 sections, 4 animals); (C) 0.1 ± 0.3 neurons (17 sections, 6 animals); (E) 61.4 ± 31.4 neurons (5 sections, 3 animals); and (F) 63.8 ± 19.9 neurons (6 sections, 3 animals). c-FOS$^+$/TH$^+$ neurons, gray; c-FOS$^+$/TH$^-$ neurons embedded within TH$^+$, black; c-FOS$^+$/TH$^-$ neurons directly surrounding TH$^+$ LC region, white. (**G**) Ascending neural circuit from preBötC. *Cdh9/Dbx1* preBötC neurons (red) provide monosynaptic excitatory input to noradrenergic LC neurons (red), which project throughout brain to promote arousal and active behaviors. Also shown is the classical circuit from preBötC rhythm-generating neurons (black) to premotorneurons in ventral respiratory group (VRG, black). (**H**) Model of preBötC with *Cdh9/Dbx1* neurons distinct from, but regulated by, rhythm-generating neurons. This provides an ascending respiratory corollary signal to the LC and on to the rest of the brain, separate from classical descending motor circuit. Hence, when breathing speeds up or is otherwise altered, *Cdh9/Dbx1* neurons activate LC to induce or maintain an aroused state. [Less direct circuits or downstream events from *Cdh9/Dbx1* neurons could also contribute to LC activation, and because LC also regulates sensory modalities (*27*, *28*), sensory alterations could also contribute to LC-induced behaviors. In addition, a direct contribution of *Cdh9/Dbx1* neurons to preBötC breathing-rhythm generation cannot be excluded, because compensatory mechanisms may obscure them.]

REFERENCES AND NOTES

1. R. P. Brown, P. L. Gerbarg, *Ann. N. Y. Acad. Sci.* **1172**, 54–62 (2009).
2. R. P. Brown, P. L. Gerbarg, *J. Altern. Complement. Med.* **11**, 711–717 (2005).
3. A. E. Nardi, R. C. Freire, W. A. Zin, *Respir. Physiol. Neurobiol.* **167**, 133–143 (2009).
4. M. B. Parshall *et al.*, *Am. J. Respir. Crit. Care Med.* **185**, 435–452 (2012).
5. J. L. Feldman, C. A. Del Negro, P. A. Gray, *Annu. Rev. Physiol.* **75**, 423–452 (2013).
6. J. C. Smith, H. H. Ellenberger, K. Ballanyi, D. W. Richter, J. L. Feldman, *Science* **254**, 726–729 (1991).
7. P. A. Gray, J. C. Rekling, C. M. Bocchiaro, J. L. Feldman, *Science* **286**, 1566–1568 (1999).
8. J. Bouvier *et al.*, *Nat. Neurosci.* **13**, 1066–1074 (2010).
9. P. A. Gray *et al.*, *J. Neurosci.* **30**, 14883–14895 (2010).
10. P. Li *et al.*, *Nature* **530**, 293–297 (2016).
11. G. Diez-Roux *et al.*, *PLOS Biol.* **9**, e1000582 (2011).
12. M. C. Picardo, K. T. Weragalaarachchi, V. T. Akins, C. A. Del Negro, *J. Physiol.* **591**, 2687–2703 (2013).
13. A. Pierani *et al.*, *Neuron* **29**, 367–384 (2001).
14. X. Wang *et al.*, *eLife* **3**, e03427 (2014).
15. C. W. Berridge, B. D. Waterhouse, *Brain Res. Brain Res. Rev.* **42**, 33–84 (2003).
16. I. R. Wickersham *et al.*, *Neuron* **53**, 639–647 (2007).
17. M. Sheng, M. E. Greenberg, *Neuron* **4**, 477–485 (1990).
18. J. G. McCall *et al.*, *Neuron* **87**, 605–620 (2015).
19. P. G. Guyenet, N. Koshiya, D. Huangfu, A. J. Verberne, T. A. Riley, *Am. J. Physiol.* **264**, R1035–R1044 (1993).
20. Y. Oyamada, D. Ballantyne, K. Mückenhoff, P. Scheid, *J. Physiol.* **513**, 381–398 (1998).
21. Z. Chen, F. L. Eldridge, P. G. Wagner, *J. Physiol.* **437**, 305–325 (1991).
22. G. Hilaire, J. C. Viemari, P. Coulon, M. Simonneau, M. Bévengut, *Respir. Physiol. Neurobiol.* **143**, 187–197 (2004).
23. K. Gleeson, C. W. Zwillich, *Am. Rev. Respir. Dis.* **145**, 453–457 (1992).
24. H. C. Kinney, B. T. Thach, *N. Engl. J. Med.* **361**, 795–805 (2009).
25. J. M. Ramirez, *Prog. Brain Res.* **209**, 91–129 (2014).
26. A. M. Valença *et al.*, *Arq. Neuropsiquiatr.* **62** (2b), 396–398 (2004).
27. M. Jiang, E. R. Griff, M. Ennis, L. A. Zimmer, M. T. Shipley, *J. Neurosci.* **16**, 6319–6329 (1996).
28. L. Hickey *et al.*, *J. Neurosci.* **34**, 4148–4160 (2014).

ACKNOWLEDGMENTS

K.Y. performed in situ screen; generated and characterized Cdh9 transgene; characterized *Cdh9/Dbx1* neuronal ablation; and performed AAV-Cre, FluoroGold, and retrograde bead injections and c-Fos experiments. L.A.S. and L.L. provided the reagents and L.A.S. injected rabies and CAV-Cre viruses. K.K. and J.L.F. provided the reagents and K.K. performed and analyzed slice electrophysiology. J.M.S. and J.R.H. provided the reagents and J.M.S. performed and analyzed ECoG recording. K.Y. analyzed all data. K.Y. and M.A.K. conceived experiments, interpreted data, and wrote the manuscript. All authors edited the manuscript. We thank X. Chen and G. Nachtrab for assistance and reagents for AAV-Cre injection, J. Zeitzer for assistance with ECoG analysis, and members of the Krasnow lab for helpful comments. This work was supported by the Howard Hughes Medical Institute (M.A.K. and L.L.), NIH grants HL70029 and HL40959 (J.L.F.), and the NIH Medical Scientist Training Program (K.Y.). M.A.K. and L.L. are investigators of the Howard Hughes Medical Institute. Data are curated and stored in the Krasnow lab at the Howard Hughes Medical Institute, Department of Biochemistry, Stanford University School of Medicine, Stanford, CA 94305, USA.

SUPPLEMENTARY MATERIALS

www.sciencemag.org/content/355/6332/1411/suppl/DC1
Materials and Methods
Figs. S1 to S15
Table S1
References (*29*–*46*)
Movie S1

21 August 2016; accepted 1 February 2017
10.1126/science.aai7984

Breathing control center neurons that promote arousal in mice
Kevin Yackle, Lindsay A. Schwarz, Kaiwen Kam, Jordan M. Sorokin, John R. Huguenard, Jack L. Feldman, Liqun Luo and Mark A. Krasnow (March 30, 2017)
Science **355** (6332), 1411-1415. [doi: 10.1126/science.aai7984]

Editor's Summary

The calming effect of breathing

The rhythmic activity of a cluster of neurons in the brainstem initiates breathing. This cluster is composed of distinct, though intermingled, subgroups of neurons. Yackle *et al.* found a small, molecularly defined neuronal subpopulation in this breathing rhythm generator that directly projects to a brain center that plays a key role in generalized alertness, attention, and stress (see the Perspective by Sheikbahaei and Smith). Removal of these cells did not affect normal breathing but left the animals unusually calm. The breathing center thus has a direct and dramatic influence on higher-order brain function.

Science, this issue p. 1411; see also p. 1370

www.sciencemag.org/content/355/6332/1411/suppl/DC1

Supplementary Materials for

Breathing control center neurons that promote arousal in mice

Kevin Yackle, Lindsay A. Schwarz, Kaiwen Kam, Jordan M. Sorokin, John R. Huguenard, Jack L. Feldman, Liqun Luo, Mark A. Krasnow*

*Corresponding author. Email: krasnow@stanford.edu

Published 31 March 2017, *Science* **355**, 1411 (2017)
DOI: 10.1126/science.aai7984

This PDF file includes:

Other Supplementary Materials for this manuscript includes the following:
(available at www.sciencemag.org/content/355/6332/1411/suppl/DC1)

Material and Methods

Animals

Dbx1-cre (*29*), Dbx1-lacZ (*13*), and Dbh-cre (*30*) have been described. Cdh9-LOSL-DTR mice are described below. Littermates of transgene-containing mice were used as wild type. Mice were housed in a 12-hour light/dark cycle with unrestricted food and water. All animal experiments were performed in accordance with national and institutional guidelines with standard precautions to minimize animal stress and the number of animals used in each experiment.

BAC transgene and transgenic line

The DTR coding sequence was placed downstream of mOrange in the Cdh9-mOrange BAC transgene, with an intervening STOP cassette containing two polyadenylation signals to prevent DTR expression. The STOP cassette (and mOrange coding sequence) was flanked by *loxP* (Cre recombination) sites (Cdh9-loxP-mOrange-Stop-loxP-DTR, abbreviated Cdh9-LOSL-DTR). The BAC transgene is designed to express mOrange in Cdh9-expressing cells, except after crossing in a Cre-expressing transgene, such as the Dbx1-Cre transgene used here, which removes the STOP cassette (including mOrange). This turns off mOrange expression in the Dbx1-Cre-expressing cells and turns on DTR in the *Cdh9*-expressing cells that also express, or previously expressed, Dbx1-Cre. Hence, in this intersectional genetic strategy with Cdh9-LOSL-DTR; Dbx1-cre animals, the Cdh9/Dbx1 double positive cells are specifically marked by DTR and can be conditionally ablated by injection of diphtheria toxin (DT) to activate DTR-induced apoptosis.

To construct the Cdh9-LOSL-DTR transgene, 500 base pair homology arms surrounding the translation start codon of *Cdh9* (chromosome 15: 16,778,101-16,778,103) were amplified by

polymerase chain reaction (PCR) using primers KY150-KY151 (see below) and KY152-KY153 and BAC RP23-318N6 as template, then cloned between BamHI and XbaI sites of pBluescript II SK+ with a KpnI-AscI-SalI polylinker added between the homology arms to generate pKY59. The mOrange stop cassette was constructed by PCR amplifying mOrange (*31*) using a 5' primer containing a *loxP* site (KY184-185) and the polyadenylation (polyA) sequence and 3' *loxP* site from MTMG (*32*) (KY186-KY140), which were inserted into the AscI site of pKY59 with a XhoI site introduced between mOrange and the polyA sequence and FseI and SpeI restriction sites introduced 3' to the distal *loxP* site to generate pKY70. The Diphtheria toxin receptor coding sequence (*33*) and the polyadenylation sequence from MTMG were PCR amplified (KY188-KY190 and KY164-KY189, respectively) and inserted between the FseI and SpeI sites of pKY70, with an EcoRI site introduced between them to create pKY73 (pBSK Cdh9-LOSL-DTR). All introduced sequences and junctions were confirmed by DNA sequencing.

For BAC recombineering, the NCI (Frederick) recombineering protocol was followed (http://ncifrederick.cancer.gov/RESEARCH/BRB/protocol.aspx). Briefly, an additional construct containing GalK for selection during BAC recombineering was generated by cloning PCR amplified GalK (KY162-KY163) into the AscI site of pKY59 between the homology arms of Cdh9 to generate pKY63. A Cdh9-containing BAC, RP23-318N6 (*34*), was electroporated into SW102 E. coli, and BAC-containing colonies selected on tetracycline and chloramphenicol containing plates. A PCR product from pKY63 (KY150-KY153) containing the GalK and Cdh9 homology arms was electroporated into heat-shocked SW102 containing the Cdh9 BAC, and selected on galactose-containing media. Colonies were streaked on MacConkey agar to identify GalK-containing colonies, and a single colony was heat-shocked and electroporated with the PCR product from pKY73 (KY150-KY153) containing the complete Cdh9-LOSL-DTR

transgene and selected on minimal media containing 2-deoxygalactose for 3 days. The final construct, containing Cdh9-LOSL-DTR inserted into the BAC (pBAC Cdh9-LOSL-DTR), was purified by BAC maxi preparation (NucleoBond BAC 100) and construct integrity was confirmed by contour-clamped homogeneous electric field electrophoresis. Purified BAC DNA was injected into eggs of FVB mice and implanted into FVB pseudopregnant females by the Stanford Transgenic Facility.

The nucleotide sequence of primers were:

KY140: 5'-CTGTTCCTGTACGGCATGG-3'

KY150: ATGATGGGATCCGTGTGTTGAAAGGATGCGGT

KY151: CATCATGGCGCGCCGGTACCTATCTTCACCTTCAGAAGGA

KY152: ATGATGGGCGCGCCGTCGACAGGACTTACAGTTGTCTTCA

KY153: CTACTATCTAGACCTTCATTTGTGAACTTTCT

KY162: CAGCAGGGCGCGCCTGTTGACAATTAATCATCGGCA

KY163: GTCGTCGGCGCGCCTCAGCACTGTCCTGCTCCTT

KY164: GAGGAGGAATTCAGCGGCCGCTCGAGCCTCGA

KY184:

GAGGAGGGCGCGCCATAACTTCGTATAGCATACATTATACGAAGTTATATGGTGAG

CAAGGGCGAGGAG

KY185: CTCCTCCTCGAGTTACTTGTACAGCTCGTCCAT

KY186: CTGCTGGGCGCGCCACTAGTGGCCGGCCATAACTTCGTATAATGTATGC

KY188: CTGCTGGAATTCTCACTAATGTATCTTATCATGTC

KY189: CTGCTGACTAGTCTCAGAAGCCATAGAGCCCAC

KY190: CAGCAGGGCCGGCCATGAAGCTGCTGCCGTCGGTGG

Recombinant viruses

All viral procedures followed the Biosafety Guidelines approved by Stanford University Administrative Panel on Laboratory Animal Care (A-PLAC) and Administrative Panel of Biosafety (APB). The following viruses were used: AAV5-CAG-FLEx^{loxP}-TVA:mCherry ($2.6x10^{12}$ particles/mL, Stanford or University of North Carolina viral core) (*35*), AAV8-CAG-FLEx^{loxP}-rabies glycoprotein ($1.3x10^{12}$ particles/mL, Stanford or University of North Carolina viral core) (*35*) or AAV1-CMV-Cre ($4.2x10^{12}$ particles/mL, University of Pennsylvania viral core). Monosynaptic rabies-GFP (deficient for rabies glycoprotein) was prepared as described previously (*36*) ($5x10^{9}$ particles/mL). Recombinant CAV-Cre was generated and purified as described previously (*37*) ($2.5x10^{12}$ particles/mL). Handling of CAV-Cre and rabies-GFP virus followed procedures approved by Stanford University Administrative Panel of Biosafety (APB) for Biosafety Level 2.

Immunostaining and 3D reconstruction of spatial patterns of gene expression in the preBötC

Postnatal day 0 brains were dissected in cold PBS, and adult brains were perfused with cold PBS and 4% paraformaldehyde. The isolated brains were fixed in 4% paraformaldehyde overnight at 4°C, then dehydrated in 30% sucrose overnight at 4°C. Cryosections (18-25 μM) were washed twice for 5 minutes in 0.1% Tween-20 in PBS, and once for 10 minutes in 0.3% Triton-X100 in PBS. Sections were blocked for 20 minutes with either 10% goat or donkey serum in 0.3% Trition-X100 PBS, then incubated overnight at 4°C in block solution containing primary antibody. Sections were washed three times for 10 minutes in 0.1% Tween-20 in PBS, then incubated for 1 hour at room temperature in block containing secondary antibody. Sections were washed in 0.1% Tween-20 in PBS and mounted in Mowiol mounting media to prevent

photobleaching. Primary antibodies used were: chicken anti-betaGAL (ICLLab CGAL-45-A-Z, diluted 1:500), rabbit anti-SST (Peninsula T-4103, 1:500), rabbit anti-NK1R (Sigma SAB4502913, 1:1000), rabbit anti-PAX2 (Covance PRB-276P, 1:500), rabbit anti-DACH1 (ProteinTech 10914-1-AP, 1:500), goat anti-LMO4 (Santa Cruz sc-11661, 1:200), rabbit anti-RFP (Clontech 632496, 1:500), goat anti-DTR (R&D AF-259, 1:20), rabbit anti-cFOS (Abcam ab7963, 1:500; Synaptic Systems, 1:500), rabbit anti-ChAT (Millipore, 1:500), armenian hamster anti-CD31 (Serotec MCA13702, 1:500), sheep anti-TH (Abcam ab113, 1:500), mouse anti-TH (Millipore mab318, 1:500). Secondary antibodies were: goat anti-rabbit 555 (Lifetech A-21429, 1:200), donkey anti-goat 488 (Lifetech A-11055, 1:200), donkey anti-goat 405 (Jackson 705-475-003, 1:200), donkey anti-mouse 488 (Lifetech A-21202, 1:250). If multiple primary antibodies of the same species were used on the same sample, each primary antibody was preincubated with cognate secondary antibody for 10 minutes and then with excess antigen to the secondary antibody before staining sections overnight at 4°C.

For 3D reconstruction of spatial expression patterns in the preBötC, serial 18 μm brain sections of P0 Cdh9-LOSL-DTR and wild type mice were immunostained for CD31, and for mOrange and Somatostatin, respectively. Scans of sequential tissue sections were manually aligned using the CD31-stained vasculature to guide the 3D reconstruction. The 3D stacks of Cdh9-mOrange stains and of Somatostatin stains were aligned to each other using anatomical landmarks (cranial nerve 7 nucleus, compact nucleus ambiguus, and ventral border of the brainstem) and Vaa3D software (*40*). We used the classical anatomical landmarks to define the preBötC (several hundred microns caudal to cranial nerve 7 nucleus, ventral to the semi-compact nucleus ambiguus, and rostral to the lateral reticular nucleus), and confirmed this anatomical localization using canonical preBötC markers Sst and Nk1r (Fig. 1 and fig. S1) (*5*).

Plethysmography, respiratory and behavioral analysis

Individual adult 8-10 week old mice were monitored in a 450 mL whole animal plethysmography chamber at room temperature (22°C) in 21% O_2 balanced with N_2 (normoxia), 10% O_2 balanced with N_2 (hypoxia), or 21% O_2/5% CO_2 balanced with N_2 (hypercapnia). Breathing was monitored by plethysmography, and other activity in the plethysmography chamber monitored by video recording, for 45 minute periods. Tidal volume, inspiratory time, and expiratory time of each breath was determined using EMKA iOX2 software; note that tidal volume values obtained in this way are only approximations of true tidal volume. Videos of mice in the plethysmography chamber were manually annotated for one of four behaviors: still sitting (no movement for greater than ~2 seconds), grooming, active (ambulating) and sleeping (stationary with eyes closed). The annotated videos were used to define behavior-specific respiratory patterns, and breathing during sleep was excluded from further analysis. Eupneic breathing was defined as 3 or more breaths in a row at respiratory rate less than 5 Hz. Sniffing was defined as 4 or more breaths in a row with a peak inspiratory flow >14 mL/sec. Sighs were defined by their characteristic augmented inspiration and waveform (*10*).

Number of experimental animals used for each condition was >10, and the same for controls, to ensure statistical power (Mead's resource equation). Their order during plethysmography recording was random and in some instances blinded. Student's t-test was used to evaluate statistical significance in comparisons of pre- and post-ablation states of respiratory (e.g., Ti, Te, and TV of each breath type) and behavioral (e.g., time spent still sitting, grooming, or active) parameters. For respiratory frequency histograms, 1000 randomly chosen data points were isolated and compared between pre- and post-ablation states, and between control and Cdh9-LOSL-DTR;Dbx1-Cre mice. Because the frequency distributions were not normal

distributions, a non-parametric test (Wilcoxon signed-rank sum test) was used to evaluate statistical significance.

Histological analysis of locus coeruleus neural activity by c-FOS immunostaining.

c-FOS is an immediate early gene that is induced by neuronal activity and standardly used as a neural activity marker in histological sections (*17*). c-FOS immunostaining of brain sections containing the locus coeruleus was done as described above. For LC analysis of animals stimulated by restraint, mice were immobilized in modified translucent polypropylene 50 mL conical tubes for 30 minutes, then placed back into their home cage for 1 hour to allow c-FOS accumulation before probing the locus coeruleus by c-FOS and TH immunostaining as described above. Note that the pattern, duration, and intensity of neural activity required to induce c-FOS expression are still incompletely understood and can differ between neuronal types; for example, in some cases neuronal spiking is sufficient for induction of c-FOS, but in others synaptic activity is required for induction (*38, 39*).

Brain activity recordings and analysis

Mice were anesthetized, and then a connector headpiece was implanted with seven ECoG cranial screw electrodes: two above frontal cortex, two above anterior parietal cortex, two above posterior parietal/occipital cortex, and one above the cerebellum for reference. The headpiece was held just above the skull while electrodes were screwed into bone, then the position of the headpiece fixed using quick-dry dental cement. Two wires were inserted into posterior neck muscles for EMG recordings. After one week to allow surgical recovery, ECoG and EMG recordings were carried out between 8:00 PM and midnight in a rectangular glass recording chamber (8x12x6 inches). Two 20 minute recording sessions (separated by 20 minutes, named trial 1 and trial 2) were done in the dark for each animal prior to Cdh9/Dbx1 neural ablation, and

then again 4-10 days after Cdh9/Dbx1 neural ablation (n = 5), using the ablation procedure described above. Similar experiments were performed for control animals pre- and post-mock ablations (n = 4). Similar experiments were also performed for the Cdh9/Dbx1 ablation animals pre- and post-ablation but with direct illumination of the recording chamber by a mercury lamp (n = 4). To evaluate the correlation between respiration and ECoG and EMG activity, ECoG, EMG and respiratory activity were synchronously recorded in the plethysmography chamber for 20 minutes, and then linear regression analyses were performed for respiratory rate and features of ECoG and EMG features. ECoG and EMG recordings were done at 2400 Hz and low-pass filtered at 1000 Hz using an RZ5 bioamp processor equipped with custom software. Signals were stored directly to disc for offline analysis using custom MATLAB scripts.

For each recording trial, ECoG was resampled and filtered between 1 and 100 Hz, de-trended to make the mean of each signal zero and normalized to unit variance (variance of entire recording = 1). The full ECoG trace was segmented into 6s epochs and Fourier transformed between 1 and 30Hz using the fast Fourier transformation. Epochs were then classified as "aroused" or "calm" based on standard criteria (*41, 42*): "aroused" segments had high Ø power, low ∂ power, small standard deviation, and high amplitude EMG, whereas "calm" segments had low Ø power, high ∂ power, large standard deviation, and low amplitude EMG. Epoch classifications were used to calculate percent time spent in calm vs. aroused states and to determine the average power spectra for each state in each recording. Statistical significance of comparisons was determined by paired-t test after verifying that normality of the data by Lilliefors test.

Targeted neuronal ablation using diphtheria toxin receptor (DTR) system

For diphtheria toxin (DT)/diphtheria toxin receptor (DTR) mediated neural ablation, mice expressing DTR in the preBötC were administered 200 ng of DT by intraperitoneal injection once a day for 3 days. Before the first injection (pre-ablation) and two days after ablation (post-ablation), mice were analyzed by plethysmography, videorecording of behavior, and ECoG as described above. When CAV-Cre and AAV-Cre viruses were used to induce DTR expression, DT injection was done as above 2-4 weeks after virus injection to allow full DTR expression.

Stereotaxic injection

Stereotaxic injections were performed in mice anaesthetized by intraperitoneal injection of 65 mg/kg ketamine and 13 mg/kg xylazine or with isofluorane. Coordinates used for the fluorogold and retrograde bead LC injections were: -5.1 mm posterior to bregma, -4.3 mm ventral from surface, ±1.0 mm from midline. Coordinates used for the preBötC were: -6.85 mm, -5.1 mm ventral from surface, ±1.3 mm from midline. Coordinates used for the rabies-GFP and CAV-Cre LC injections were: 0.8 mm posterior to lambda, -3.2 mm ventral, ±0.8 mm from midline. Injection sites were confirmed by the restricted expression of TVA:mCherry and rabies-GFP in tyrosine-hydroxylase-expressing LC neurons (fig. S12).

Retrograde neuronal tracing

For retrograde bead tracing, P35-56 Cdh9-LOSL-DTR mice were stereotaxically injected into the LC with 50 nL of fluorogold or retrograde beads (*43*). Four to seven days after injection, animals were euthanized and tissue was processed as above and analyzed for retrograde labeling as follows. Serial preBötC tissue sections (25 μm) were immunostained for mOrange to detect Cdh9-mOrange expression, and fluorogold and retrograde beads were detected by autofluorescence.

For monosynaptic retrograde tracing using rabies-GFP, adult P42-56 Cdh9-mOrange;Dbh-Cre mice were anesthetized with ketamine and xylazine, then 500 nL of a 1:1 mixture of AAV8 CAG-FLEx^{loxP}-rabies glycoprotein and AAV5 CAG-FLEx^{loxP}-TVA:mCherry were stereotaxically injected into the left LC at the coordinates given above. Two weeks later, 300-500 nL of modified rabies-GFP virus (RV*d*G) (*35*) was injected into the same position using the procedure described above. After recovery, mice were housed in a biosafety-level-2 (BSL2) facility for 4-5 days before harvesting and analysis as above. Tracing efficiency using this technique was 15-30% (0-6 rabies-GFP traced Cdh9-mOrange neurons among the ~20-40 Cdh9-mOrange neurons present in each 25 μm sagittal preBötC section), similar to that in other applications of the technique (*44*).

To estimate the number of preBötC neurons that directly project to the locus coeruleus (LC), we used the rabies tracing data and considered only traced projections from the contralateral preBötC (because rabies-traced neurons within the ipsilateral ventrolateral medulla fell outside the preBötC region defined by the canonical preBötC marker Somatostatin, as shown in fig. S13). From the number of retrogradely labeled rabies-eGFP positive neurons in the contralateral preBötC (~4 scored rabies-eGFP positive neurons per 25-35 μm preBötC section x 8 sections per preBötC = ~30-35 rabies-eGFP positive neurons per preBötC), and assuming a 10-30% tracing efficiency by the rabies technique, we estimate ~100-350 preBötC neurons project to the contralateral LC. Because ~63% of traced preBötC neurons are Cdh9$^+$ (see Results), we calculate ~60-220 Cdh9$^+$ preBötC neurons project to the LC. This estimate suggests that many or all of the ~175 Cdh9/Dbx1 preBötC neurons project to the LC.

Single cell electrophysiology in preBötC brain slices

Rhythmic 550-μm-thick transverse medullary slices containing the preBötC and cranial nerve

XII (XIIn) from neonatal Cdh9-mOrange or Cdh9-mOrange;Dbx1-LacZ mice (P0-5) were prepared as described (*45*). Slices were cut in ACSF containing (in mM): 124 NaCl, 3 KCl, 1.5 $CaCl_2$, 1 $MgSO_4$, 25 $NaHCO_3$, 0.5 NaH_2PO_4, and 30 D-glucose, equilibrated with 95% O_2 and 5% CO_2 (4°C, pH=7.4). For recording, extracellular K^+ was raised to 9 mM and allowed to equilibrate for 30 min. Generalized preBötC neural activity, as a measure of inspiratory activity, was recorded from either XIIn roots or as population activity directly from the preBötC using suction electrodes, full-wave rectified, and digitally integrated after blanking perfusion artifacts. The mOrange-expressing neurons recorded were located ventral or slightly ventrolateral to the nucleus ambiguus. For whole cell and loose-patch recordings, intracellular solution contained (in mM): 135 KGluconate, 1.1 EGTA, 5 NaCl, 0.1 $CaCl_2$, 10 HEPES, 2 MgATP, 0.3 Na_3GTP, 0.1% Lucifer Yellow. In voltage clamp recordings, holding potential was -65 mV, and experiments in which variations in series and input resistance exceeded the initial value by 25% were discarded. For loose-patch recordings, action potential (AP) shape was monitored to detect stability of the patch. All electrophysiological recordings were performed with a MultiClamp 700A or 700B, filtered at 2–4 kHz and digitized at 10 kHz. For Dbx1-lacZ expression typing, 0.1% Lucifer Yellow was allowed to diffuse into the cell for >15 minutes to mark the neurons that had been patched, and then the slices were placed in 4% paraformaldehyde overnight, washed, and stored at 4°C in PBS until beta-galactosidase (LacZ) immunostaining. For immunostaining, slices were incubated for 3 days in chicken anti-betaGAL (ICLLab CGAL-45-A-Z, diluted 1:500) containing 10% donkey serum then washed (3 times for 2 hours in 0.1% Tween-20 in PBS) and incubated in donkey anti-chicken 649 (Jackson Immunoresearch 703-495-155, diluted 1:500) containing 10% donkey block for 48 hours. Slices were cleared for visualization in SCALE (*46*) for several days.

To evaluate the statistical significance of the apparent association between action potential bursts of the $Cdh9^+$ inspiratory-associated neurons and inspiratory bursts of the preBotC (monitored by cXIIn or preBötC population recordings), we compared the results to those using Monte-Carlo simulations of randomly distributed preBötC inspiratory bursts. Action potential bursts of $Cdh9^+$ inspiratory-associated neurons were defined as three or more action potentials whose frequency was two standard deviations greater than the mean frequency or were a burst of excitatory postsynaptic potential that depolarized the neuron for longer than 100 ms. The time difference (Δt) between the center of the $Cdh9^+$ burst and the center of the nearest preBötC inspiratory burst was measured and compared to the Δt for same number of random events generated by Monte Carlo simulation. Each simulation was run 1000 times and a distribution of mean Δt's was obtained. For all neurons identified as inspiratory-associated, the actual mean Δt was outside the 95% confidence interval of the simulated data, indicating that the association between action potential bursts and inspiratory bursts is unlikely a chance occurrence.

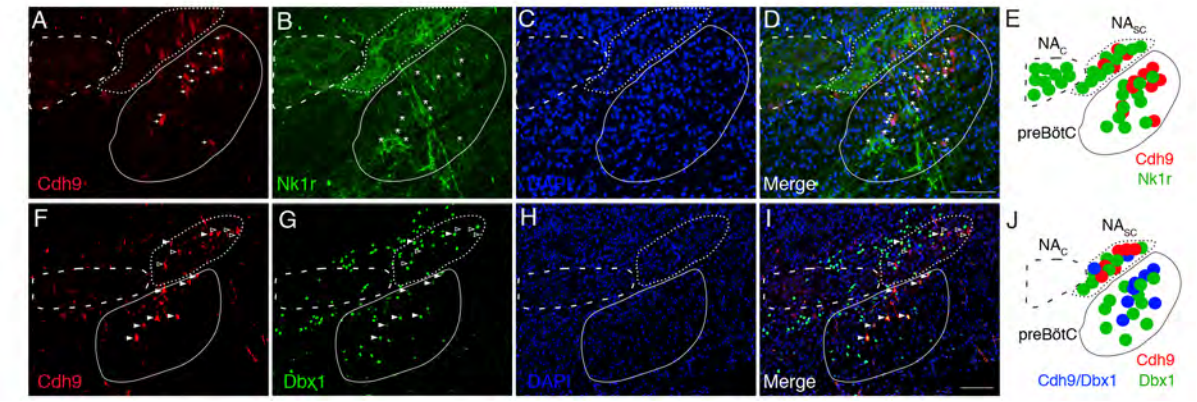

Fig. S1. Localization of Cdh9/DBx1 neurons relative to canonical preBötC marker NK1R and nucleus ambiguus. A-D, Sagittal section of ventrolateral medulla of P0 Cdh9-LOSL-DTR mouse immunostained to show Cdh9 expression (mOrange, red) and canonical preBötC marker NK1R (green), and stained with DAPI (blue) to show nuclei. Although both genes are selectively expressed in preBötC region (outline) and intermingled, few preBötC neurons co-express both genes (3.9%; 7 double positive of 179 Cdh9 preBötC neurons scored). Note that both the compact region (NA_c, dashed outline, large nuclei) and the semicompact region of nucleus ambiguous (NA_{sc}, dotted outline, immediately caudal to NA_c) also express NK1R, and that most Cdh9-expressing neurons (arrows) localize to the preBötC region defined by NK1R-expressing neurons (asterisks) ventral to the NA_{sc}. Similar results obtained using nucleus ambiguus markers Dach1 and choline acetyl transferase (ChAT) (data not shown). Bar, 100 µm. **E**, Schematic showing intermingling of Cdh9 (red) and NK1R expressing (green) neurons in preBötC and their relationship to the two anatomical subdivisions of the nucleus ambiguus (NA_c and NA_{sc}) . **F-I**, Representative sagittal section of the ventrolateral medulla of P0 Cdh9-LOSL-DTR;Dbx1-lacZ mouse immunostained to show Cdh9 expression (mOrange, red) and Dbx1 expression (beta-galactosidase, green), and stained with DAPI (blue) to show nuclei. Note that most Cdh9/Dbx1 double-positive neurons (filled arrowheads) localize to the preBötC ventral to the NAsc. Open

arrowheads, Cdh9 single-positive neurons. Bar, 100 μm. **J**, Schematic summary of localization of Cdh9/Dbx1 neurons in preBötC region.

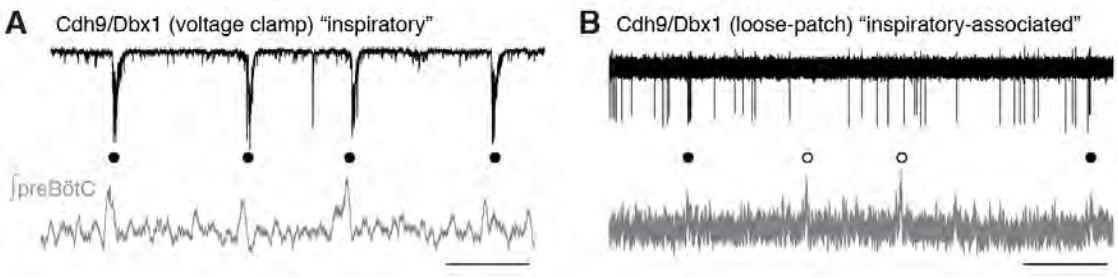

Fig. S2. Continuous electrophysiology recording of Cdh9/Dbx1 neurons. A,B, Voltage clamp (A) or loose-patch (B) recordings (black) of individual Cdh9/Dbx1 preBötC neurons in preBötC slice preparations, with simultaneous recording of preBötC activity (gray, either cranial nerve 12 or preBötC population activity). Circles, inspiratory events (shown by preBötC activity); filled circles, inspiratory events associated with action potential burst of recorded Cdh9/Dbx1 neuron. Note neuron in A (neuron 1, Table S1) shows action potential bursts during all inspiratory events ("inspiratory pattern"), whereas neuron in B (neuron 3) shows more widespread activity with bursts during only some inspiratory events ("inspiratory-associated pattern"). Bars, 5 sec.

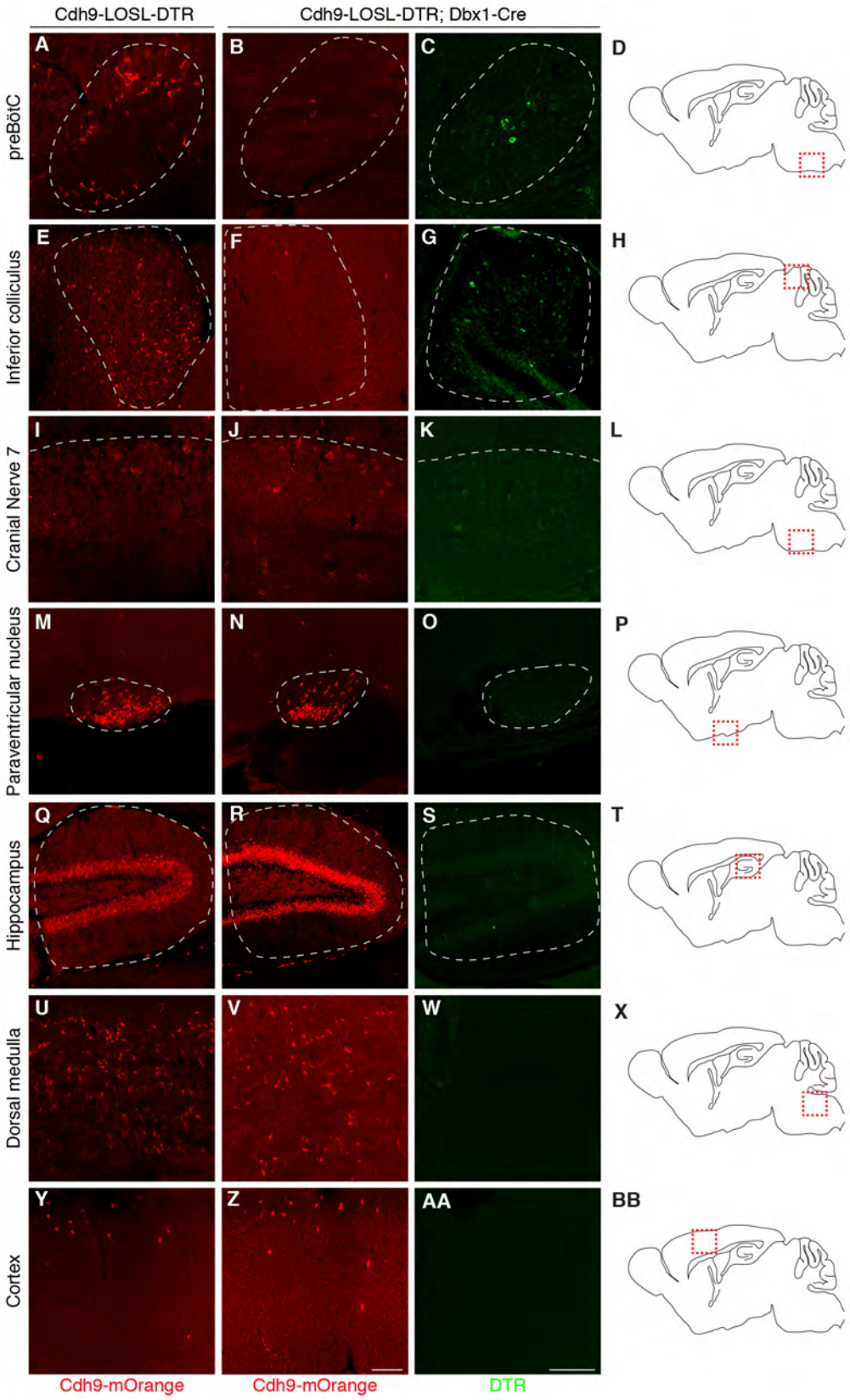
Cdh9-LOSL-DTR
Cdh9-LOSL-DTR; Dbx1-Cre
preBötC
Inferior colliculus
Cranial Nerve 7
Paraventricular nucleus
Hippocampus
Dorsal medulla
Cortex
A
B
C
D
E
F
G
H
I
J
K
L
M
N
O
P
Q
R
S
T
U
V
W
X
Y
Z
AA
BB
Cdh9-mOrange
Cdh9-mOrange
DTR

Fig. S3. Specificity of intersectional genetic expression of diphtheria toxin receptor in Cdh9-LOSL-DTR; Dbx1-cre mice. Sagittal sections of seven Cdh9-mOrange expressing brain regions (positions indicated in schematics at right) from adult (~P35) Cdh9-LOSL-DTR (A,E,I,M,Q,U,Y) or Cdh9-LOSL-DTR;Dbx1-Cre (B,C,F,G,J,K,N,O,R,S,V,W,Z,AA) mouse brains and immunostained for either mOrange to show Cdh9 expression (red) or DTR (green). Dbx1-Cre eliminates mOrange expression in many cells and turns on DTR expression in preBötC (A-C) and inferior colliculus (E-H) but not the other brain regions. Bars, 100 μm.

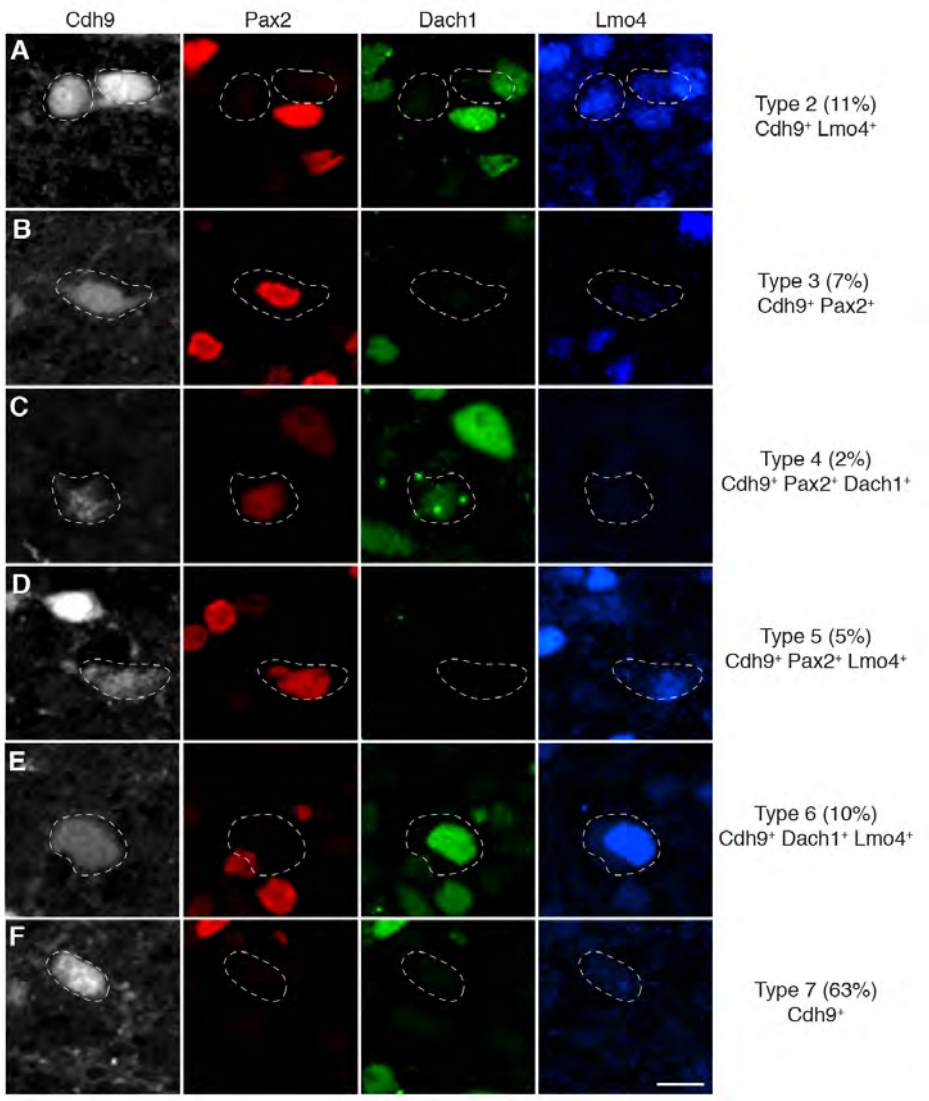

Fig. S4. Selective loss of mOrange expression in preBötC Cdh9/Dbx1 neurons in Cdh9-LOSL-DTR;Dbx1-cre mice. Close-up of regions within preBötC of P0 Cdh9-LOSL-DTR;Dbx1-Cre quadruple immunostained to show Cdh9 expression (mOrange, white), PAX2 (red), DACH1 (green), and LMO4 (blue). Six of the seven Cdh9-expressing preBötC neuronal subtypes (A-F, Types 2 -7) (*7*) were detected in the proportions indicated (n=139 Cdh9-expressing neurons scored in 2 animals) Cdh9/Dbx1 preBötC neurons (Type 1 neurons), which also express all three of the markers shown (PAX2, DACH1, and LMO4) and are the most

abundant subtype (>50%) were only rarely detected (<1%) in this intersectional cross, as expected because Dbx1-Cre deletes the mOrange cassette specifically in Type 1 neurons. Bar, 10 μm.

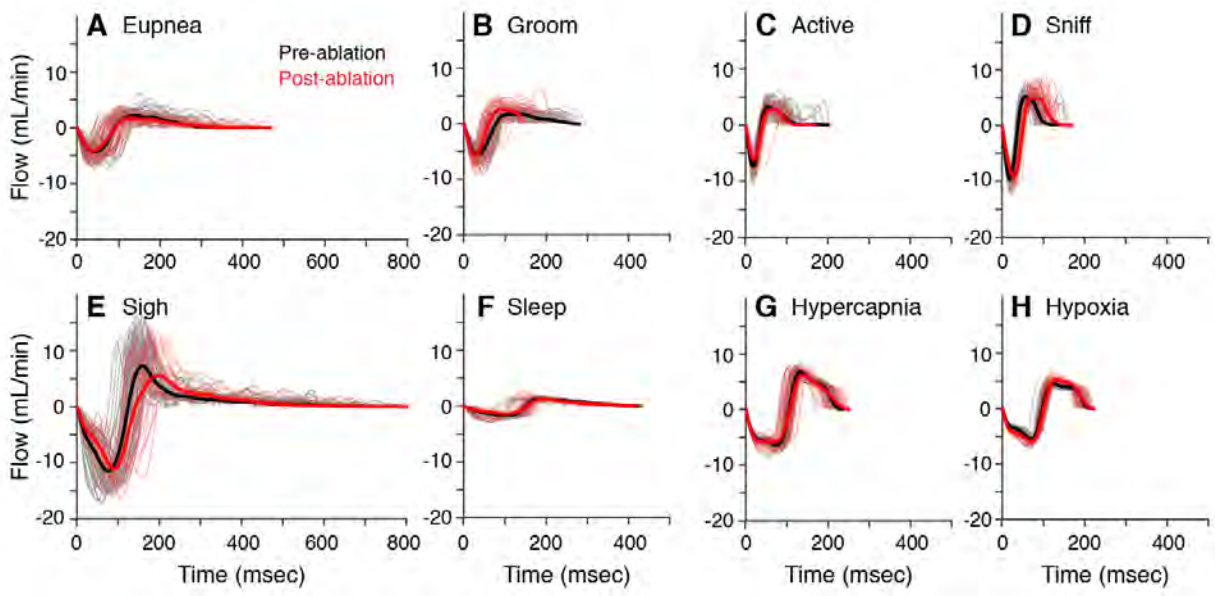

Fig. S5. Analysis of respiratory rhythms following Cdh9/Dbx1 neuronal ablation.

Comparison of standard (A, eupneic) and normal variant respiratory waveforms (B-H) in awake (A-E) and asleep (F) animals in room air (A-F) or under 5% CO_2 (G, hypercapnia) or 10% O_2 (H, hypoxia) in ~P49-56 Cdh9-LOSL-DTR;Dbx1-Cre mice before (pre-ablation, black) and 2 days after ablation (post-ablation, red) of Cdh9/Dbx1 neurons by DT injection. Each panel shows 50 randomly selected examples of each waveform from a single Cdh9-LOSL-DTR;Dbx1-Cre mouse before (pre-ablation, thin black lines) and after ablation (post-ablation, thin red lines) along with the average pre and post-ablation waveform (thick black and red lines).

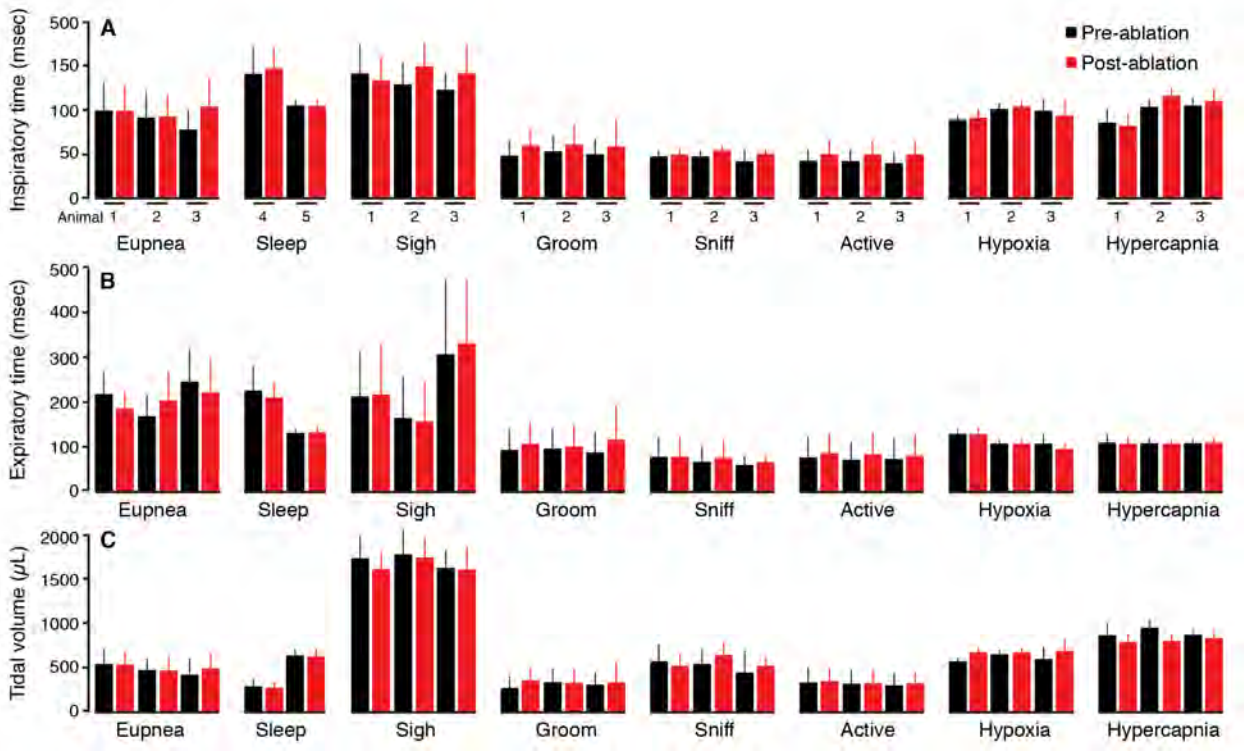

Fig. S6. Effect of Cdh9/Dbx1 neuron ablation on breathing patterns.

A-C, Inspiratory (A) and expiratory (B) times and tidal volume (C) of the eight breath types indicated (see Fig. S5) in a ~40 minute plethysmography assay of ~P35-56 Cdh9-LOSL-DTR;Dbx1-Cre mice before (black, pre-ablation) and 2 days after (red, post-ablation) DT injection to ablate Cdh9/Dbx1 neurons. Breaths analyzed during hypoxia (10% oxygen) and hypercapnia (5% carbon dioxide) challenges exclude breaths that occurred during active periods. Each pair of bars shows the mean and standard deviation of all breaths of each type (range 23 - 10222 breaths) from one animal (labeled 1-5 below in A). None of the differences in respiratory parameters following ablation (pooled individual data) were statistically significant (all p-values > 0.19).

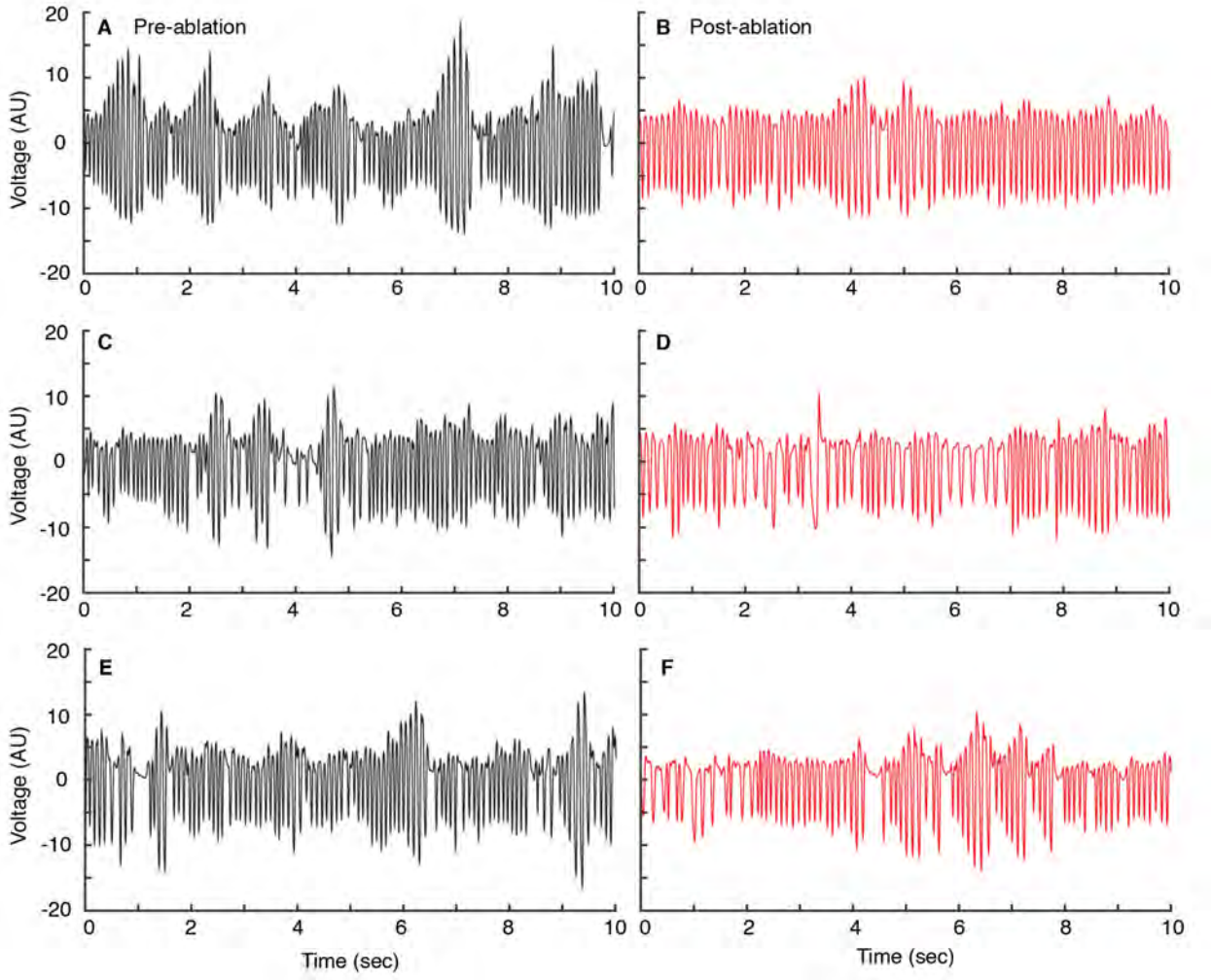

Fig. S7. Additional plethysmography data from actively behaving animals. Voltage values acquired during randomly selected 10-second intervals of a 40-minute plethysmography trace before (A,C,E, black) and after (B,D,F, red) diphtheria toxin mediation ablation of Cdh9/Dbx1 neurons. All recordings are from the same mouse. Note the breath morphology during active behavior does not change after ablation.

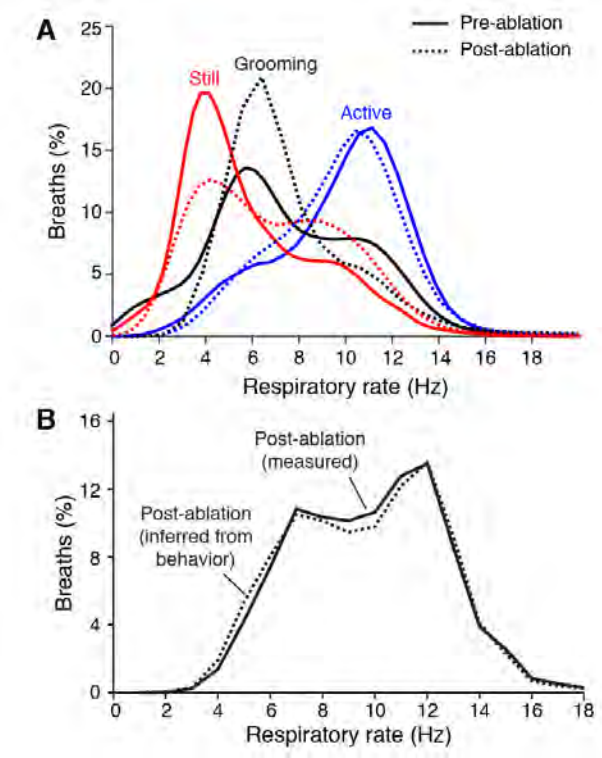

Fig. S8. The change in respiratory rates following Cdh9/Dbx1 neural ablation can be accounted for by changes in behavior. **A**, Distribution of respiratory rates (RR, in Hz) for each of the indicated behaviors (still sitting, red; grooming, black; active, blue) in ~P35-56 Cdh9-LOSL-DTR;Dbx1-Cre mice (n = 5) during 40 minute assay of breathing and behavior in plethysmography chamber, before (solid lines) and 2 days after (dotted lines) DT injection to ablate Cdh9/Dbx1 preBötC neurons. Note differences in respiratory rates for the different behaviors, with lower respiratory rates associated with calm behaviors (calm sitting, grooming) and higher rates associated with arousal (active) behavior. **B**, Measured composite RR histogram (solid line) as above from Cdh9-LOSL-DTR; Dbx1-cre mice with Cdh9/Dbx1 neurons ablated (as in Fig. 2), and an inferred RR histogram (dashed line) generated by combining RR histograms of the individual behaviors of control mice (wild type, Cdh9-LOSL-DTR or Dbx1-

Cre) proportionally to the time spent by Cdh9-LOSL-DTR;Dbx1-cre ablated animals performing each behavior (Fig. 2C). The inferred RR histogram closely matches the measured histogram.

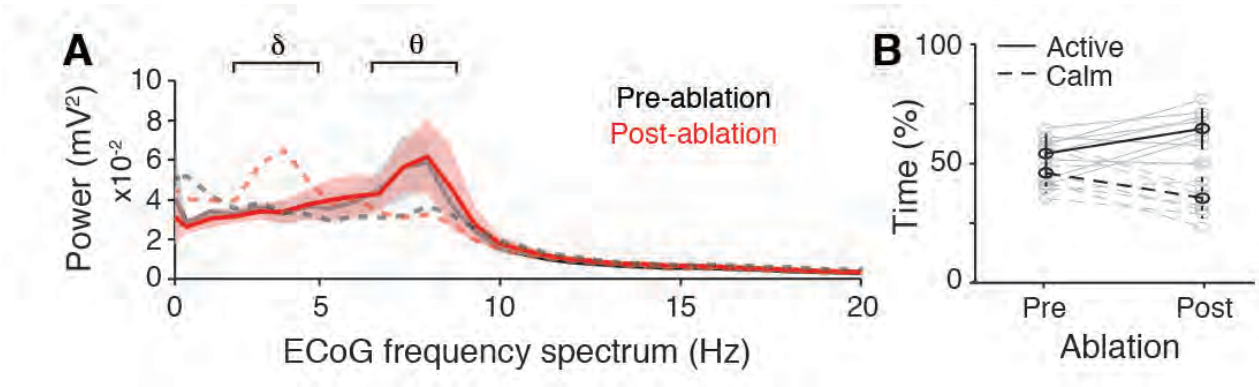

Fig. S9. Ablation of Cdh9/Dbx1 preBötC neurons does not affect arousal behavior in a brightly illuminated chamber. A, Fast Fourier transform power spectral analysis of ECoG activity of Cdh9-LOSL-DTR;Dbx1-Cre mice (n = 4) before (black solid line) or 4-10 days after (red solid line) Cdh9/Dbx1 neural ablation in a 20-minute assay (trial 1) in an illuminated recording chamber. Note increased arousal that is unaffected by Cdh9/Dbx1 neural ablation, as indicated by increased power in the theta range (8-9 Hz) relative to ECoG recordings before (black dashed line) and after (red dashed line) Cdh9/Dbx1 neural ablation in the same assay without chamber illumination (reproduced from Fig. 2F and H). δ, delta wave. θ, theta wave. V, voltage. Plots show average values (lines) ± S.E.M (shading, shown only for the illumination condition). **B**, Quantification of time spent in active (solid lines) and calm (dashed lines) behavioral states defined by EMG and ECoG recordings (see fig. S15) of four Cdh9-LOSL-DTR;Dbx1-Cre mice before (pre-ablation) and 4-10 days after neural ablation (post-ablation) in a two 20-minute assays in an illuminated recording chamber. Unlike Fig. 2G, the Cdh9/Dbx1 ablated animals do not show increased calm behavior after Cdh9/Dbx1 ablation when assayed in an illuminated recording chamber, and instead show increased active behavior. P-value for change in active periods pre versus post ablation: p=0.0177 and calm periods: p=0.0177.

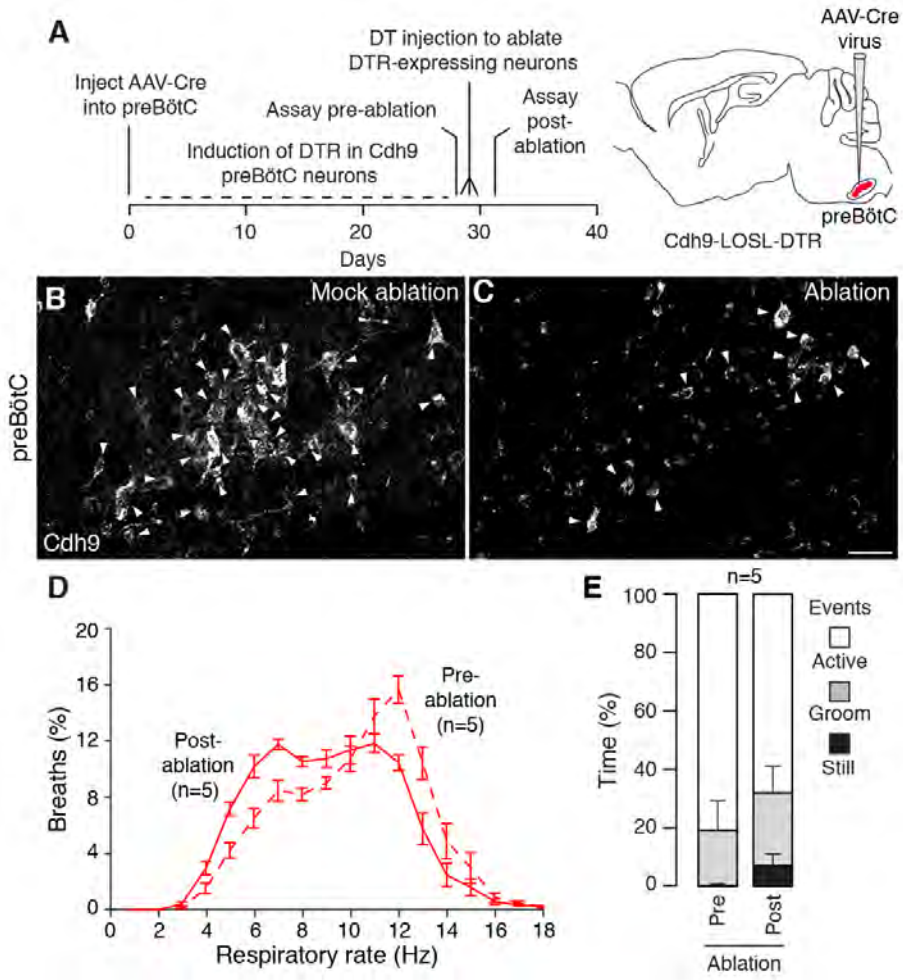

Fig. S10. Effect on breathing and behavior of ablation of Cdh9 preBötC neurons. A, Ablation scheme. AAV-Cre virus is injected bilaterally into preBötC of adult Cdh9-LOSL-DTR mice. After 4 weeks to allow virus uptake, Cre expression, and Cre-mediated recombination to induce diphtheria toxin receptor (DTR) expression in neurons expressing Cdh9 (red), the Cdh9-expressing, preBötC neurons were ablated by injection of 3 doses of diphtheria toxin (DT). Two days later animals were assayed by plethysmography. **B, C** Cdh9-mOrange expression (white) in preBötC 2 days after DT injection of control (no AAV-Cre) mock-ablation (B) or experimental (AAV-Cre injected) Cdh9 preBotC neuron ablated (C) Cdh9-LOSL-DTR mice. Note reduction

in Cdh9-expressing cells (arrowheads) in the AAV-Cre injected animal (C). Bar, 50 μm. **D**, Distribution of respiratory rates in a 40 min period (as in Fig. 2B) of AAV-Cre injected Cdh9-LOSL-DTR adult (n = 5) before (pre-ablation, dashed red line) or 2 days after (post-ablation, solid red line) diphtheria toxin injection. Note shift in distribution toward lower respiratory rates following ablation ($p=1.2x10^{-17}$, Wilcoxon rank sum of 1000 random breaths), similar to that observed after genetic ablation of Cdh9/Dbx1 neurons (Fig. 2B). **E**, Behavioral analysis (as in Fig. 2C) of mice in D shown as percent of period spent active (white), grooming (grey) or still sitting (black). p-value of difference between pre and post-ablation behaviors: active (0.07), grooming (0.23), and still sitting (0.03).

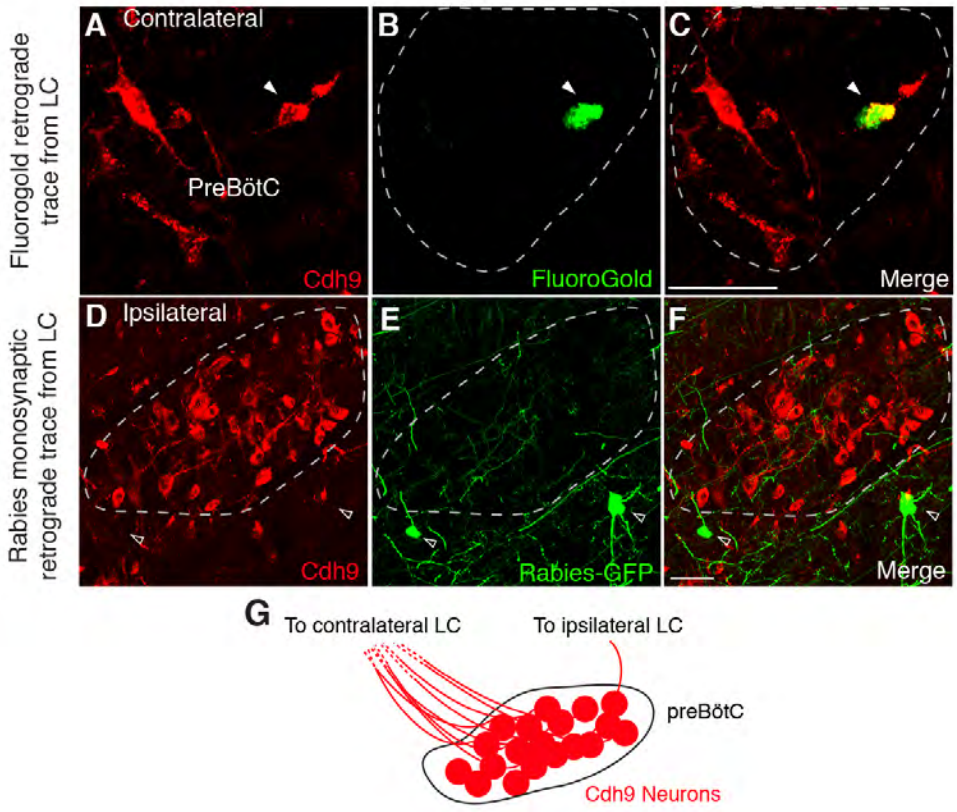

Fig. S11. Identification and characterization of Cdh9 preBötC neuronal projections to locus coeruleus by retrograde tracing. A-C, preBötC (dashed circle) of adult Cdh9-LOSL-mOrange mouse with Fluorogold retrograde tracing beads (green) injected into contralateral LC 7 days earlier and then harvested and immunostained for Cdh9-expressing neurons (mOrange, red). Note preBötC Cdh9-expressing neuron labeled with Fluorogold retrograde trace (arrowhead). Similar results were obtained in three separate experiments. Bar, 50 µm. **D-F.** Rabies virus monosynaptic retrograde tracing from dopamine beta hydroxylase (Dbh)-expressing LC neurons as in Fig. 3A-C. Section through ipsilateral (D-F) preBötC of adult Cdh9-LOSL-DTR;Dbh-Cre with rabies-GFP and helper virus injected into an LC 5-7 days earlier and then harvested and immunostained to show Cdh9-expressing neurons (mOrange, red). Note, rabies-GFP (green) is not in ipsilateral Cdh9-expressing preBötC neurons and is instead found in

neurons (open arrowheads) just outside preBötC (dashed line). Bars, 50 μm. **G**, Schematic of preBötC showing most Cdh9-expressing neurons project directly to contralateral rather than ipsilateral LC.

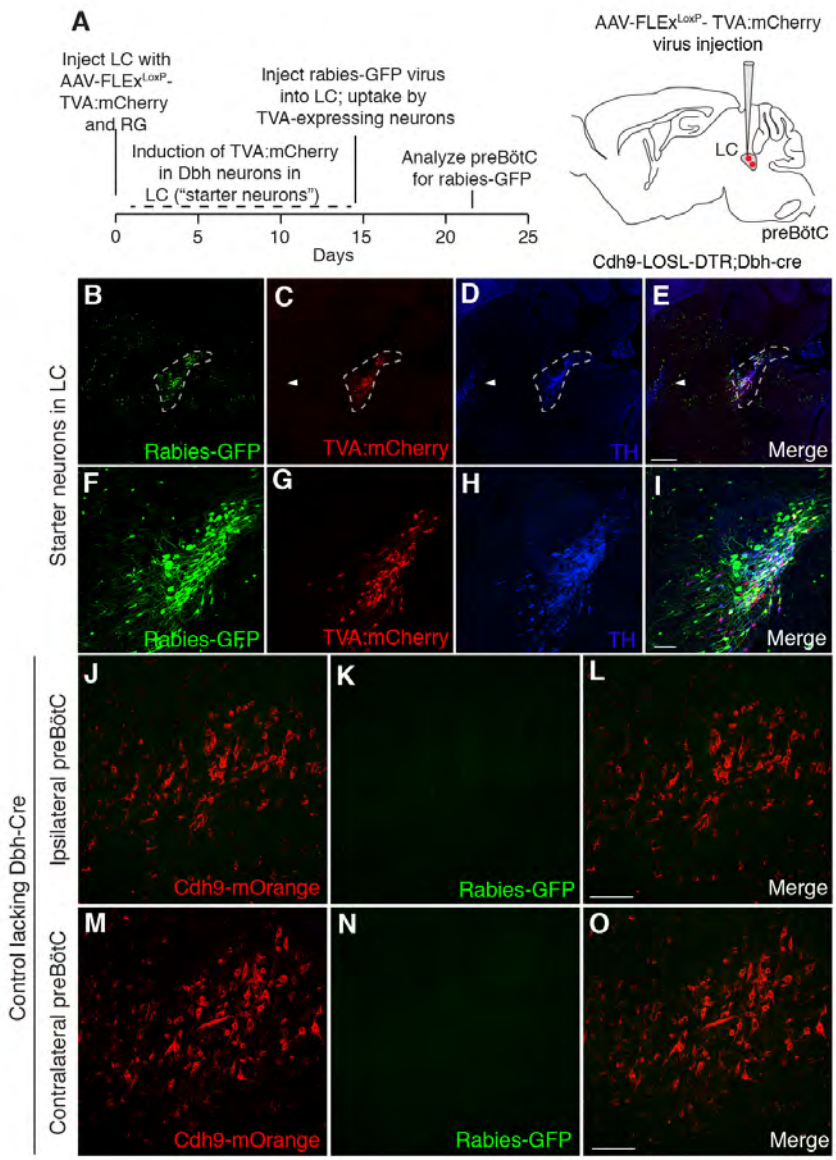

Fig. S12. Specificity controls for rabies-GFP monosynaptic retrograde neural circuit tracing from LC. A, Retrograde tracing scheme. Unilateral stereotaxic injection of AAV-CAG-FLEx^{loxP}-TVA:mCherry virus and AAV-CAG-FLEx^{loxP}-rabies glycoprotein into LC of adult Cdh9-LOSL-DTR;Dbh-Cre mice results in virus uptake and Cre-mediated recombination in Dbh-expressing (noradrenergic) LC neurons, which turns on TVA-mCherry expression. After 2 weeks to allow accumulation of TVA-mCherry, the same LC is injected with a modified rabies

virus that specifically infects only TVA-expressing neurons and expresses GFP. 5-7 days later, preBötC is analyzed for rabies-GFP expression, which indicates retrograde trace from Dbh-expressing neurons in LC. **B-I**, Starter neurons in LC for retrograde monosynaptic tracing. Section through LC (E-F) and close-up of encircled region (G-I) of adult Cdh9-LOSL-DTR;Dbh-Cre mouse 5-7 days after injection with modified rabies virus and imaged for rabies-GFP (green; C, G), TVA:mCherry (red; D,H), and canonical LC marker tyrosine hydroxylase (TH immunostain, blue; E, I). Note that LC neurons expressing Rabies-GFP and TVA-mCherry also express the canonical LC marker tyrosine hydroxylase (encircled), whereas nearby TH-expressing neurons (arrowhead) do not express mCherry or Rabies-GFP. Bars, 400 μm (C-F), 100 μm (G-J). **J-O**, Ipsilateral (J-L) and contralateral (M-O) preBötC of adult Cdh9-LOSL-DTR control animal (lacking Dbh-Cre) immunostained for Cdh9 (red) and GFP (green) 5-7 days after rabies-GFP virus injection into LC. No GFP-expressing neurons are seen in either ipsilateral or contralateral preBötC. Bar, 100 μm.

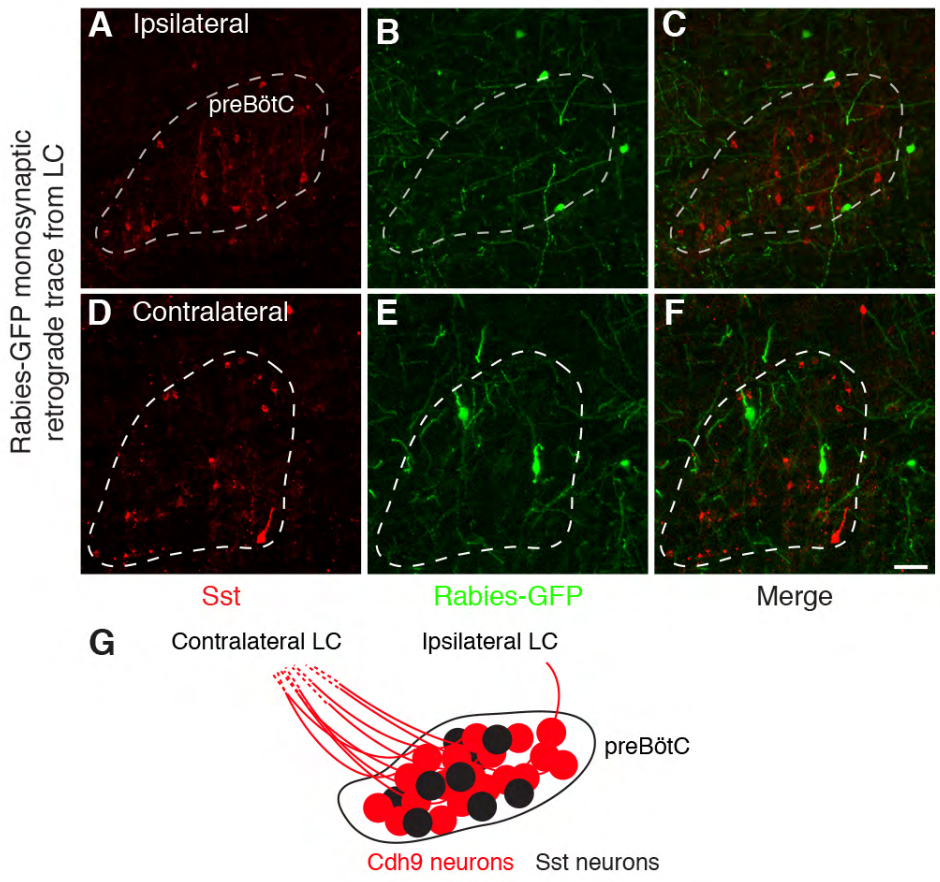

Fig. S13. Rabies virus monosynaptic retrograde tracing from locus coeruleus labels few somatostatin-expressing neurons in preBötC. Rabies-GFP virus monosynaptic retrograde trace (rabies-GFP, green) from locus coeruleus dopamine beta hydroxylase (Dbh)-expressing (noradrenergic) neurons in Cdh9-LOSL-DTR;Dbh-Cre mice as in Fig. 3A-C and Fig. S11, except that sections through ipsilateral (**A-C**) and contralateral (**D-F**) preBötC were immunostained for canonical preBötC marker Sst (red). Note that none of the rabies-GFP-expressing cells shown also express SST. Quantification showed that 0 of 35 contralateral, and 1 of 51 (2%) ipsilateral GFP-expressing neurons scored were SST-positive. On the ipsilateral side, a small cluster of GFP-expressing neurons was present outside and ventral to the preBötC SST-expressing neurons, along with some more scattered GFP-expressing neurons (not shown). Bars,

50 µm. **G**, Summary showing predominance of contralateral projections of Cdh9-expressing preBötC neurons to LC, and very few ipsilateral projections or projections from SST-expressing preBötC neurons to LC.

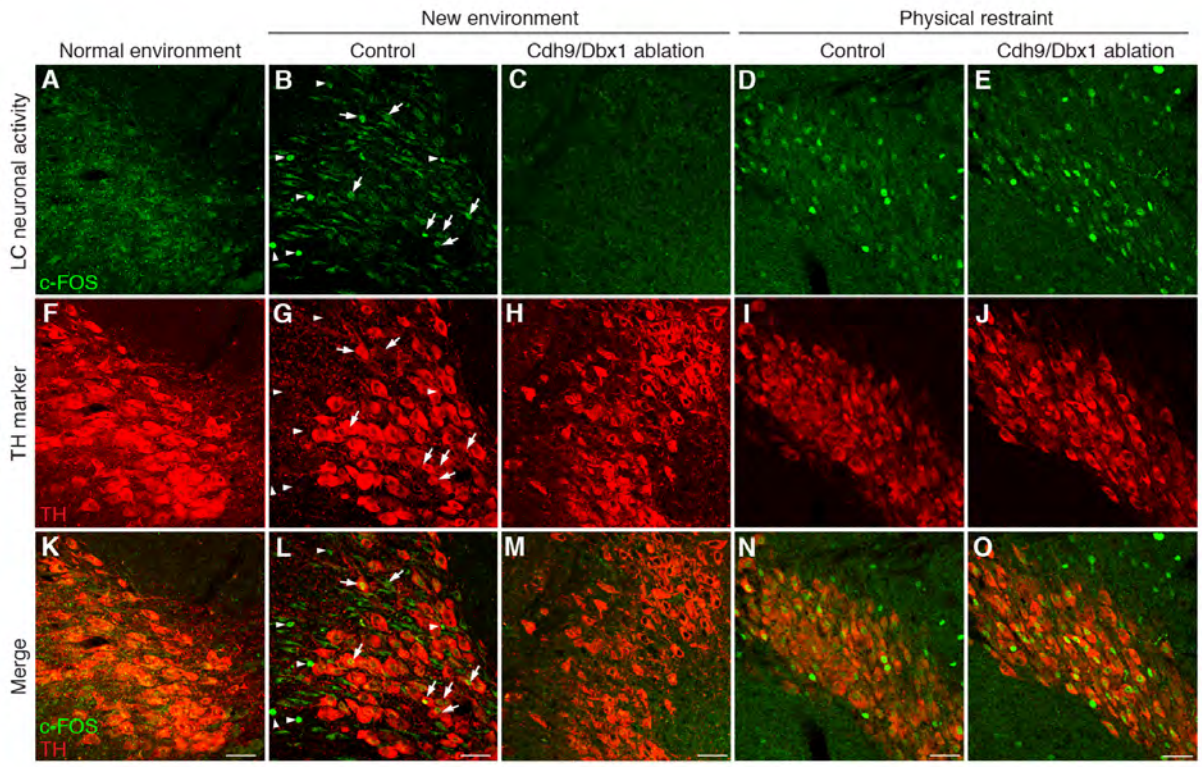

Fig. S14. Effect of Cdh9/Dbx1 neuron ablation on activity of tyrosine hydroxylase-expressing (TH^+) LC neurons. LC neuron activity assays by c-FOS immunostaining of wild type, control, and Cdh9/Dbx1-ablated animals were done as in Fig. 4, but with co-stains for tyrosine hydroxylase (TH, red; F-J) and merged images (K-O) to examine effect on activity of the Dbh-expressing (noradrenergic) subset of LC neurons, which also express TH and are thought to mediate arousal (*15*). **A-E,** c-FOS immunostaining (green) of LC of adult wild type mouse in normal environment (home cage, A), or of control (wild type, Cdh9-LOSL-DTR, or Dbx1-Cre mice, B,D) and Cdh9/Dbx1-ablated mice (Cdh9-LOSL-DTR;Dbx1-cre mice 2 days after DT injection, C,E) 1 hour after placing in new environment (plethysmography chamber, B,C) or after 30 minute of physical restraint in a conical tube (D,E). **F-J,** Tyrosine hydroxylase (TH) co-stains (red) of A-E. **K-O,** Merged images. Note c-FOS is induced in TH^+ LC neurons

(arrows) as well as some TH^- neurons embedded among the TH^+ LC neurons (arrow) and some TH^- neurons surrounding them (arrowheads) in control animals in new environment (L) and in both control (N) and Cdh9/Dbx1-ablated animals (O) under physical constraint, but not in Cdh9/Dbx1-ablated animals in new environment (M). Bars, 50 μm.

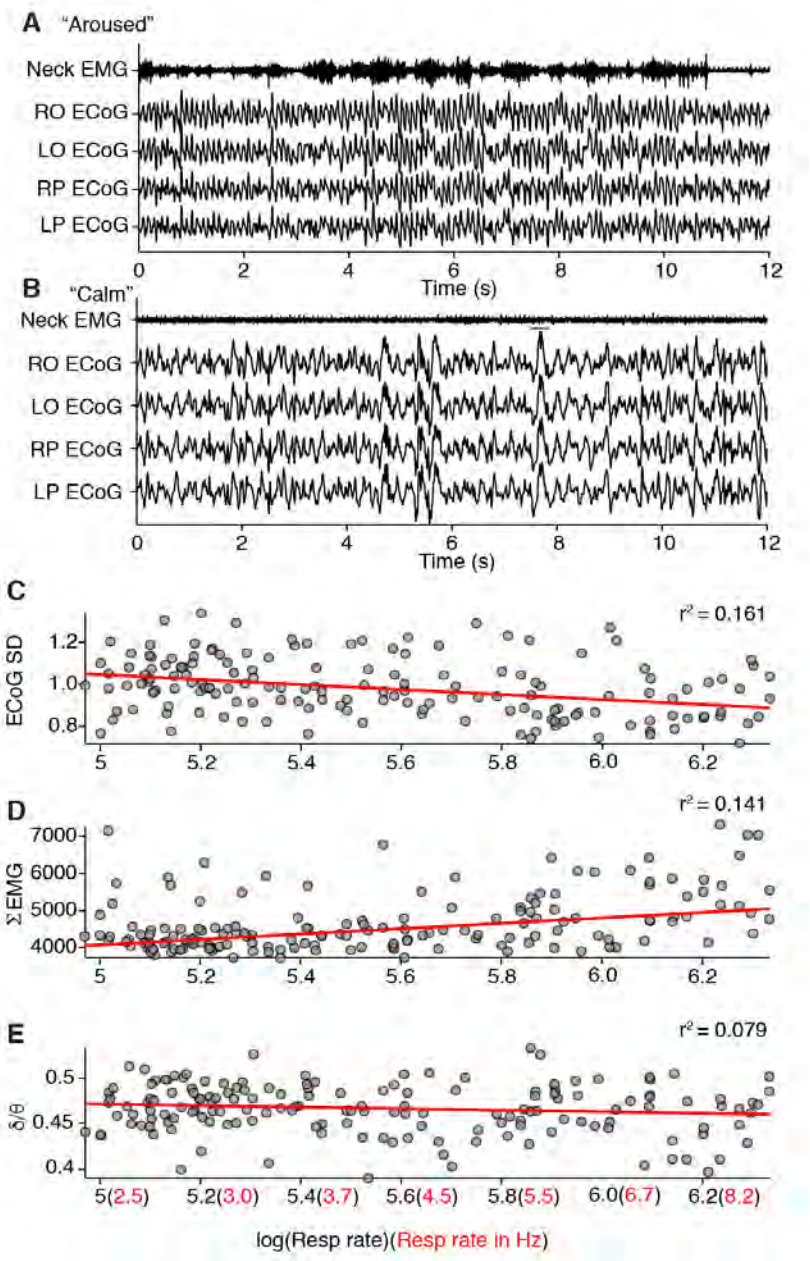

Fig. S15. Active vs. calm electromyographic (EMG) and electrocorticographic (ECoG) signatures. Example "aroused" (A) and "calm" (B) periods identified by EMG activity traces (top trace, recorded from posterior neck muscles) and corresponding ECoG activity traces (bottom traces, recorded bilaterally from indicated brain regions) in a Cdh9-LOSL-DTR;Dbx1-Cre mouse pre-ablation. Periods scored as "aroused" had high EMG activity and theta (6.5-9 Hz)

brain waves and low variance ECoG signatures, whereas periods scored as "calm" had low EMG activity and delta (1-4 Hz) brain waves, occasional K-complexes (bar), and high variance ECoG signatures. **C-E**, Regression analysis showing relationship between respiratory rate (plotted as log(RR) but values also shown in Hz) and either ECoG standard deviation (C), summated EMG activity (D), or ratio of brain delta/theta wave powers (δ/θ) (E) of a wild type adult mouse. Each point represents the average RR and respective ECoG, EMG, or delta/theta wave power values for a six second epoch in a 20 minute trial. Red line, regression fit. Note that RR is highest during active behavior defined by low ECoG SD, high EMG activity, and low (δ/θ). P-values for each regression: 0.00002 (C), 0.00000 (D), 0.12 (E).

Neuron	Animal	Slice	preBötC marker		Firing pattern				
			Cdh9	Dbx1	Inspiratory	Associated	Tonic	Sporadic	Silent
1	6	1	+	+	+				
2	7	1	+	+		+			
3	14	1	+	+		+			
4	14	1	+	+		+			
5	4	7	+	+				+	
6	5	9	+	-	+				
7	6	1	+	-	+				
8	10	G	+	-	+				
9	1	1	+	-		+			
10	10	G	+	-					+
11	13	J	+	-					+
12	4	7	+	n.d.	+				
13	8	E	+	n.d.	+				
14	8	E	+	n.d.	+				
15	15	1	+	n.d.	+				
16	2	1	+	n.d.		+			
17	6	1	+	n.d.		+			
18	12	I	+	n.d.			+		
19	15	1	+	n.d.			+		
20	15	1	+	n.d.				+	
21	3	1	+	n.d.				+	
22	5	9	+	n.d.					+
23	5	9	+	n.d.					+
24	9	F	+	n.d.					+
25	11	H	+	n.d.					+
26	12	I	+	n.d.					+

Table S1. Electrophysiological activity patterns of Cdh9-mOrange neurons in preBötC slices. 26 Cdh9-mOrange-positive neurons were recorded in preBötC in vitro slice preparations from either Cdh9-mOrange or Cdh9-mOrange;Dbx1-LacZ mice (n = 15). Neuron, neuron identification number; Animal, animal from which neuron derived; Slice, slice number of recorded neuron; Cdh9, Cdh9-mOrange expression of neuron; Dbx1, Dbx1-lacZ expression of neuron (n.d., not determined because neuron either did not carry Dbx1-LacZ transgene or did not show Lucifer yellow expression); Firing pattern, neural activity pattern relative to generalized preBötC activity (Inspiratory, consistently fired with each preBötC inspiratory burst; Associated, fired with some but not all preBötC inspiratory bursts).

Movie S1. Representative video of Cdh9-LOSL-DTR;Dbx1-Cre mouse behavior before (left) and after (right) Cdh9/Dbx1 neural ablation. The videos are of the same mouse and are from the first 2 minutes of a plethysmography assay.

References and Notes

1. R. P. Brown, P. L. Gerbarg, Yoga breathing, meditation, and longevity. *Ann. N. Y. Acad. Sci.* **1172**, 54–62 (2009). doi:10.1111/j.1749-6632.2009.04394.x Medline

2. R. P. Brown, P. L. Gerbarg, Sudarshan Kriya yogic breathing in the treatment of stress, anxiety, and depression. Part II—clinical applications and guidelines. *J. Altern. Complement. Med.* **11**, 711–717 (2005). doi:10.1089/acm.2005.11.711 Medline

3. A. E. Nardi, R. C. Freire, W. A. Zin, Panic disorder and control of breathing. *Respir. Physiol. Neurobiol.* **167**, 133–143 (2009). doi:10.1016/j.resp.2008.07.011 Medline

4. M. B. Parshall, R. M. Schwartzstein, L. Adams, R. B. Banzett, H. L. Manning, J. Bourbeau, P. M. Calverley, A. G. Gift, A. Harver, S. C. Lareau, D. A. Mahler, P. M. Meek, D. E. O'Donnell, American Thoracic Society Committee on Dyspnea, An official American Thoracic Society statement: Update on the mechanisms, assessment, and management of dyspnea. *Am. J. Respir. Crit. Care Med.* **185**, 435–452 (2012). doi:10.1164/rccm.201111-2042ST Medline

5. J. L. Feldman, C. A. Del Negro, P. A. Gray, Understanding the rhythm of breathing: So near, yet so far. *Annu. Rev. Physiol.* **75**, 423–452 (2013). doi:10.1146/annurev-physiol-040510-130049 Medline

6. J. C. Smith, H. H. Ellenberger, K. Ballanyi, D. W. Richter, J. L. Feldman, Pre-Bötzinger complex: A brainstem region that may generate respiratory rhythm in mammals. *Science* **254**, 726–729 (1991). doi:10.1126/science.1683005 Medline

7. P. A. Gray, J. C. Rekling, C. M. Bocchiaro, J. L. Feldman, Modulation of respiratory frequency by peptidergic input to rhythmogenic neurons in the preBötzinger complex. *Science* **286**, 1566–1568 (1999). doi:10.1126/science.286.5444.1566 Medline

8. J. Bouvier, M. Thoby-Brisson, N. Renier, V. Dubreuil, J. Ericson, J. Champagnat, A. Pierani, A. Chédotal, G. Fortin, Hindbrain interneurons and axon guidance signaling critical for breathing. *Nat. Neurosci.* **13**, 1066–1074 (2010). doi:10.1038/nn.2622 Medline

9. P. A. Gray, J. A. Hayes, G. Y. Ling, I. Llona, S. Tupal, M. C. D. Picardo, S. E. Ross, T. Hirata, J. G. Corbin, J. Eugenín, C. A. Del Negro, Developmental origin of preBötzinger complex respiratory neurons. *J. Neurosci.* **30**, 14883–14895 (2010). doi:10.1523/JNEUROSCI.4031-10.2010 Medline

10. P. Li, W. A. Janczewski, K. Yackle, K. Kam, S. Pagliardini, M. A. Krasnow, J. L. Feldman, The peptidergic control circuit for sighing. *Nature* **530**, 293–297 (2016). doi:10.1038/nature16964 Medline

11. G. Diez-Roux, S. Banfi, M. Sultan, L. Geffers, S. Anand, D. Rozado, A. Magen, E. Canidio, M. Pagani, I. Peluso, N. Lin-Marq, M. Koch, M. Bilio, I. Cantiello, R. Verde, C. De Masi, S. A. Bianchi, J. Cicchini, E. Perroud, S. Mehmeti, E. Dagand, S. Schrinner, A. Nürnberger, K. Schmidt, K. Metz, C. Zwingmann, N. Brieske, C. Springer, A. M. Hernandez, S. Herzog, F. Grabbe, C. Sieverding, B. Fischer, K. Schrader, M. Brockmeyer, S. Dettmer, C. Helbig, V. Alunni, M.-A. Battaini, C. Mura, C. N. Henrichsen, R. Garcia-Lopez, D. Echevarria, E. Puelles, E. Garcia-Calero, S. Kruse, M. Uhr, C. Kauck, G. Feng, N. Milyaev, C. K. Ong, L. Kumar, M. Lam, C. A. Semple, A.

Gyenesei, S. Mundlos, U. Radelof, H. Lehrach, P. Sarmientos, A. Reymond, D. R. Davidson, P. Dollé, S. E. Antonarakis, M.-L. Yaspo, S. Martinez, R. A. Baldock, G. Eichele, A. Ballabio, A high-resolution anatomical atlas of the transcriptome in the mouse embryo. *PLOS Biol.* **9**, e1000582 (2011). doi:10.1371/journal.pbio.1000582 Medline

12. M. C. Picardo, K. T. Weragalaarachchi, V. T. Akins, C. A. Del Negro, Physiological and morphological properties of *Dbx1*-derived respiratory neurons in the pre-Botzinger complex of neonatal mice. *J. Physiol.* **591**, 2687–2703 (2013). doi:10.1113/jphysiol.2012.250118 Medline

13. A. Pierani, L. Moran-Rivard, M. J. Sunshine, D. R. Littman, M. Goulding, T. M. Jessell, Control of interneuron fate in the developing spinal cord by the progenitor homeodomain protein Dbx1. *Neuron* **29**, 367–384 (2001). doi:10.1016/S0896-6273(01)00212-4 Medline

14. X. Wang, J. A. Hayes, A. L. Revill, H. Song, A. Kottick, N. C. Vann, M. D. LaMar, M. C. D. Picardo, V. T. Akins, G. D. Funk, C. A. Del Negro, Laser ablation of Dbx1 neurons in the pre-Bötzinger complex stops inspiratory rhythm and impairs output in neonatal mice. *eLife* **3**, e03427 (2014). doi:10.7554/eLife.03427 Medline

15. C. W. Berridge, B. D. Waterhouse, The locus coeruleus-noradrenergic system: Modulation of behavioral state and state-dependent cognitive processes. *Brain Res. Brain Res. Rev.* **42**, 33–84 (2003). doi:10.1016/S0165-0173(03)00143-7 Medline

16. I. R. Wickersham, D. C. Lyon, R. J. O. Barnard, T. Mori, S. Finke, K.-K. Conzelmann, J. A. T. Young, E. M. Callaway, Monosynaptic restriction of transsynaptic tracing from single, genetically targeted neurons. *Neuron* **53**, 639–647 (2007). doi:10.1016/j.neuron.2007.01.033 Medline

17. M. Sheng, M. E. Greenberg, The regulation and function of c-*fos* and other immediate early genes in the nervous system. *Neuron* **4**, 477–485 (1990). doi:10.1016/0896-6273(90)90106-P Medline

18. J. G. McCall, R. Al-Hasani, E. R. Siuda, D. Y. Hong, A. J. Norris, C. P. Ford, M. R. Bruchas, CRH engagement of the locus coeruleus noradrenergic system mediates stress-induced anxiety. *Neuron* **87**, 605–620 (2015). doi:10.1016/j.neuron.2015.07.002 Medline

19. P. G. Guyenet, N. Koshiya, D. Huangfu, A. J. Verberne, T. A. Riley, Central respiratory control of A5 and A6 pontine noradrenergic neurons. *Am. J. Physiol.* **264**, R1035–R1044 (1993). Medline

20. Y. Oyamada, D. Ballantyne, K. Mückenhoff, P. Scheid, Respiration-modulated membrane potential and chemosensitivity of locus coeruleus neurones in the in vitro brainstem-spinal cord of the neonatal rat. *J. Physiol.* **513**, 381–398 (1998). doi:10.1111/j.1469-7793.1998.381bb.x Medline

21. Z. Chen, F. L. Eldridge, P. G. Wagner, Respiratory-associated rhythmic firing of midbrain neurones in cats: Relation to level of respiratory drive. *J. Physiol.* **437**, 305–325 (1991). doi:10.1113/jphysiol.1991.sp018597 Medline

22. G. Hilaire, J. C. Viemari, P. Coulon, M. Simonneau, M. Bévengut, Modulation of the respiratory rhythm generator by the pontine noradrenergic A5 and A6 groups in rodents.

Respir. Physiol. Neurobiol. **143**, 187–197 (2004). doi:10.1016/j.resp.2004.04.016 Medline

23. K. Gleeson, C. W. Zwillich, Adenosine stimulation, ventilation, and arousal from sleep. *Am. Rev. Respir. Dis.* **145**, 453–457 (1992). doi:10.1164/ajrccm/145.2_Pt_1.453 Medline

24. H. C. Kinney, B. T. Thach, The sudden infant death syndrome. *N. Engl. J. Med.* **361**, 795–805 (2009). doi:10.1056/NEJMra0803836 Medline

25. J. M. Ramirez, The integrative role of the sigh in psychology, physiology, pathology, and neurobiology. *Prog. Brain Res.* **209**, 91–129 (2014). doi:10.1016/B978-0-444-63274-6.00006-0 Medline

26. A. M. Valença, A. E. Nardi, M. A. Mezzasalma, I. Nascimento, F. L. Lopes, W. A. Zin, M. Versiani, Clonidine in respiratory panic disorder subtype. *Arq. Neuropsiquiatr.* **62** (2b), 396–398 (2004). doi:10.1590/S0004-282X2004000300004 Medline

27. M. Jiang, E. R. Griff, M. Ennis, L. A. Zimmer, M. T. Shipley, Activation of locus coeruleus enhances the responses of olfactory bulb mitral cells to weak olfactory nerve input. *J. Neurosci.* **16**, 6319–6329 (1996). Medline

28. L. Hickey, Y. Li, S. J. Fyson, T. C. Watson, R. Perrins, J. Hewinson, A. G. Teschemacher, H. Furue, B. M. Lumb, A. E. Pickering, Optoactivation of locus ceruleus neurons evokes bidirectional changes in thermal nociception in rats. *J. Neurosci.* **34**, 4148–4160 (2014). doi:10.1523/JNEUROSCI.4835-13.2014 Medline

29. F. Bielle, A. Griveau, N. Narboux-Nême, S. Vigneau, M. Sigrist, S. Arber, M. Wassef, A. Pierani, Multiple origins of Cajal-Retzius cells at the borders of the developing pallium. *Nat. Neurosci.* **8**, 1002–1012 (2005). doi:10.1038/nn1511 Medline

30. S. Gong, M. Doughty, C. R. Harbaugh, A. Cummins, M. E. Hatten, N. Heintz, C. R. Gerfen, Targeting Cre recombinase to specific neuron populations with bacterial artificial chromosome constructs. *J. Neurosci.* **27**, 9817–9823 (2007). doi:10.1523/JNEUROSCI.2707-07.2007 Medline

31. N. C. Shaner, R. E. Campbell, P. A. Steinbach, B. N. G. Giepmans, A. E. Palmer, R. Y. Tsien, Improved monomeric red, orange and yellow fluorescent proteins derived from *Discosoma* sp. red fluorescent protein. *Nat. Biotechnol.* **22**, 1567–1572 (2004). doi:10.1038/nbt1037 Medline

32. M. D. Muzumdar, B. Tasic, K. Miyamichi, L. Li, L. Luo, A global double-fluorescent Cre reporter mouse. *Genesis* **45**, 593–605 (2007). doi:10.1002/dvg.20335 Medline

33. M. Saito, T. Iwawaki, C. Taya, H. Yonekawa, M. Noda, Y. Inui, E. Mekada, Y. Kimata, A. Tsuru, K. Kohno, Diphtheria toxin receptor-mediated conditional and targeted cell ablation in transgenic mice. *Nat. Biotechnol.* **19**, 746–750 (2001). doi:10.1038/90795 Medline

34. K. Osoegawa, M. Tateno, P. Y. Woon, E. Frengen, A. G. Mammoser, J. J. Catanese, Y. Hayashizaki, P. J. de Jong, Bacterial artificial chromosome libraries for mouse sequencing and functional analysis. *Genome Res.* **10**, 116–128 (2000). Medline

35. L. A. Schwarz, K. Miyamichi, X. J. Gao, K. T. Beier, B. Weissbourd, K. E. DeLoach, J. Ren, S. Ibanes, R. C. Malenka, E. J. Kremer, L. Luo, Viral-genetic tracing of the input-output

organization of a central noradrenaline circuit. *Nature* **524**, 88–92 (2015). doi:10.1038/nature14600 Medline

36. F. Osakada, E. M. Callaway, Design and generation of recombinant rabies virus vectors. *Nat. Protoc.* **8**, 1583–1601 (2013). doi:10.1038/nprot.2013.094 Medline

37. E. J. Kremer, S. Boutin, M. Chillon, O. Danos, Canine adenovirus vectors: An alternative for adenovirus-mediated gene transfer. *J. Virol.* **74**, 505–512 (2000). doi:10.1128/JVI.74.1.505-512.2000 Medline

38. P. Schoenenberger, D. Gerosa, T. G. Oertner, Temporal control of immediate early gene induction by light. *PLOS ONE* **4**, e8185 (2009). doi:10.1371/journal.pone.0008185 Medline

39. S. M. Luckman, R. E. Dyball, G. Leng, Induction of c-fos expression in hypothalamic magnocellular neurons requires synaptic activation and not simply increased spike activity. *J. Neurosci.* **14**, 4825–4830 (1994). Medline

40. H. Peng, A. Bria, Z. Zhou, G. Iannello, F. Long, Extensible visualization and analysis for multidimensional images using Vaa3D. *Nat. Protoc.* **9**, 193–208 (2014). doi:10.1038/nprot.2014.011 Medline

41. M. Kreuzer, S. Polta, J. Gapp, C. Schuler, E. F. Kochs, T. Fenzl, Sleep scoring made easy—Semi-automated sleep analysis software and manual rescoring tools for basic sleep research in mice. *MethodsX* **2**, 232–240 (2015). doi:10.1016/j.mex.2015.04.005 Medline

42. P. Karasinski, L. Stinus, C. Robert, A. Limoge, Real-time sleep-wake scoring in the rat using a single EEG channel. *Sleep* **17**, 113–119 (1994). Medline

43. B. R. Schofield, Retrograde axonal tracing with fluorescent markers. *Curr. Protoc. Neurosci.* **43**, 1.17.1–1.17.24 (2008). doi:10.1002/0471142301.ns0117s43 Medline

44. E. M. Callaway, L. Luo, Monosynaptic circuit tracing with glycoprotein-deleted rabies viruses. *J. Neurosci.* **35**, 8979–8985 (2015). doi:10.1523/JNEUROSCI.0409-15.2015 Medline

45. K. Kam, J. W. Worrell, W. A. Janczewski, Y. Cui, J. L. Feldman, Distinct inspiratory rhythm and pattern generating mechanisms in the preBötzinger complex. *J. Neurosci.* **33**, 9235–9245 (2013). doi:10.1523/JNEUROSCI.4143-12.2013

46. H. Hama, H. Kurokawa, H. Kawano, R. Ando, T. Shimogori, H. Noda, K. Fukami, A. Sakaue-Sawano, A. Miyawaki, Scale: A chemical approach for fluorescence imaging and reconstruction of transparent mouse brain. *Nat. Neurosci.* **14**, 1481–1488 (2011). doi:10.1038/nn.2928 Medline